



January 2014

Development Of Novel Max Phase Composites

Thomas Jacob Hammann

Follow this and additional works at: <https://commons.und.edu/theses>

Recommended Citation

Hammann, Thomas Jacob, "Development Of Novel Max Phase Composites" (2014). *Theses and Dissertations*. 1658.
<https://commons.und.edu/theses/1658>

This Thesis is brought to you for free and open access by the Theses, Dissertations, and Senior Projects at UND Scholarly Commons. It has been accepted for inclusion in Theses and Dissertations by an authorized administrator of UND Scholarly Commons. For more information, please contact zeinebyousif@library.und.edu.

DEVELOPMENT OF NOVEL MAX PHASE COMPOSITES

by

Thomas Jacob Hammann

Bachelor of Science, University of North Dakota, 2013

A Thesis

Submitted to the Graduate Faculty

of the

University of North Dakota

In partial fulfillment of the requirements

for the degree of

Master of Science

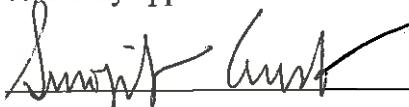
Grand Forks, North Dakota

December

2014

Copyright 2014 Thomas J. Hammann


This thesis, submitted by Thomas Jacob Hammann in partial fulfillment of the requirements for the Degree of Master of Sciences in Mechanical Engineering from the University of North Dakota, has been read by the Faculty Advisory Committee under whom the work has been done and is hereby approved.



Surojit Gupta, Ph.D.

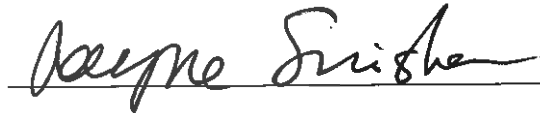


Matthew Cavalli, Ph.D., P.E.



Bishu Bandyopadhyay, Ph.D

This Thesis is being submitted by the appointed advisory committee as having met all of the requirements of the Graduate School at the University of North Dakota and is hereby approved.



Wayne Swisher, Ph.D



Date

PERMISSION

Title DEVELOPMENT OF NOVEL MAX PHASE COMPOSITES
Department Mechanical Engineering
Degree Masters of Science

In presenting this thesis in partial fulfillment of the requirements for a graduate degree from the University of North Dakota, I agree that the library of this University shall make it freely available for inspection. I further agree that permission for extensive copying for scholarly purposes may be granted by the professor who supervised my thesis work or, in his absence, by the Chairperson of the department or the Dean of the Graduate School. It is understood that any copying or publication or other use of this thesis or part thereof for financial gain shall not be allowed without my written permission. It is also understood that due recognition shall be given to me and the University of North Dakota in any scholarly use which may be made of any material in my thesis.

Thomas Jacob Hammann

December 19, 2014

TABLE OF CONTENTS

LIST OF FIGURES	vii
ABSTRACT.....	x
CHAPTER	
I. INTRODUCTION	1
1.1 MAX Phases and MAX-Metal Composites.....	1
1.2 MAX Phase Unit Cell Variations	4
1.3 Elastic Properties of MAX Phases.....	7
1.4 Machinability and Mechanical Behavior of MAX Phases	8
1.5 MAX Phase-Metal Composites	10
1.6 MAX Phase-Epoxy Composites	12
II. SYNTHESIS OF NOVEL MAX-Al(ALUMINUM) COMPOSITES....	14
2.1 Fabrication Processes.....	14
2.2 Results and Discussion	15
2.3 Conclusions.....	20
III. SYNTHESIS OF NOVEL MAX-Sn(TIN) COMPOSITES.....	21
3.1 Fabrication Process	21
3.2 Results and Discussion	23

3.3 Conclusions.....	27
IV. SYNTHESIS OF NOVEL MAX-EPOXY COMPOSITES	28
4.1 Fabrication Processes.....	28
4.2 Results and Discussion	29
4.3 Conclusions.....	32
V. FUTURE STUDIES.....	33
5.1 Synthesis of Novel MAX-Al(Aluminum)-Sn(Tin) Composites...	33
5.2 Manufacturing Details	34
APPENDIX.....	38
Status of journal publications.....	38
Contributed presentations during Master's degree	38
REFERENCES	
Chapter 1	41
Chapter 2.....	43
Chapter 3.....	46
Chapter 4.....	49

LIST OF FIGURES

1.1. Periodic Table	2
1.2. Illustrated variations of the MAX phases, where a, b, and c represent the unit cells for M_2AX (211), M_3AX_2 (312), and M_4AX_3 (413), respectively.....	4
1.3. Picture of MAX phase Ti_2AlC after hit with a steel hammer; picture's width is about 20cm. Picture courtesy of 3-ONE-2.	10
2.1. XRD profiles of different composites of Al- Ti_3SiC_2	16
2.2. Secondary Electron SEM micrographs of etched surfaces of sintered, (a) Al, (b) 5 vol% Ti_3SiC_2 , (c) 10 vol% Ti_3SiC_2 and (d) Backscattered (BSE) image of the same region, (e) 20 vol% Ti_3SiC_2 , and (f) BSE image of the same region, in Al matrix (Al- Ti_3SiC_2 composites).....	17
2.3. Secondary Electron images of Al(80)- Ti_3SiC_2 (20) composites at, (a) low, and (b) higher magnification and (c) BSE image of the higher magnification region.	18
2.4. Plots of Al-Matrix properties, (a) change in porosity versus different vol% of Ti_3SiC_2 additions in the Al matrix, (b) compressive stress versus displacement profiles of different Al matrix composites, and (c) the effect of Ti_3SiC_2 additions on the yield strength (Y1 axis) and hardness (Y2 axis) of Al matrix composites, (d) actual densities of the composites.	19
3.1. XRD profiles of, (a) Sn, (b) Sn(95)- Ti_3SiC_2 (5), (c) Sn(90)- Ti_3SiC_2 (10), (d) Sn(80)- Ti_3SiC_2 (20), (e) Sn(70)- Ti_3SiC_2 (30).	23

3.2. SE SEM of (a) Sn(70)-Ti ₃ SiC ₂ (30), (b) Sn(80)-Ti ₃ SiC ₂ (20), (c) Sn(90)-Ti ₃ SiC ₂ (10), (d) Sn(100)	24
3.3. Porosity change with the increase of Ti ₃ SiC ₂ vol%	25
3.4. Compressive strength profiles of Sn-matrix composites (a) and comparison of compressive strength to the hardness of the composites (b).	26
4.1. SEM micrographs of epoxy-matrix composites, (a) epoxy-32.6 vol% Ti ₃ SiC ₂ in SE mode, (b) BSE image of the same region, and (c) epoxy-71.6 vol% Ti ₃ SiC ₂ in SE mode, and (d) BSE image of the same region.	30
4.2a. Plot of compressive strength versus displacement.....	31
4.2b. Ultimate Yield Strength (UYS) (Y1 axis) and hardness (Y2 axis) versus different volume fraction additions of Ti ₃ SiC ₂ in the epoxy matrix.....	32
5.1. Relative density of HP Al-Sn-MAX.....	35
5.2. Various manufacturing methods' effect on porosity.	36

ACKNOWLEDGMENTS

I am grateful to my colleagues, Ryan R. Johnson, and M Faisal Riyad, for without them this work would not have been possible.

In addition I would like to express my sincerest gratitude to my professors at the University of North Dakota for all of the aid and support I received during my studies.

To my sister Sara Jean Hammann; for her unparalleled ability to overcome adversity and continue to progress in life while raising two beautiful daughters, Bryjah and Remi. It is because of you, while redefining the role of an older sibling, you showed me the world as I see it now and made this all possible.

ABSTRACT

The $M_{n+1}AX_n$ (MAX) phases are thermodynamically stable nanolaminates which display unusual, and in some cases unique, properties. There currently exist over 60 MAX phases in the literature. These phases are named because they possess a $M_{n+1}AX_n$ chemistry, where n is equal to 1, 2, or 3, M is an early transition metal element, A is an A-group element, and X is carbon and/or nitrogen. MAX phases are layered hexagonal (space group $D4h-P63/mmc$) with two formula units per unit cell. The MAX phase material group has high damage tolerance, thermal shock resistance, resistant to creep, lubricious, readily machinable, and has Vickers hardness values of 2-8 GPa which is anomalously soft for transitional metal carbides and nitrides. Some of the MAX phases are also oxidation resistant. The properties of the MAX phases make them very appealing to scientists and engineers for many different structural applications.

CHAPTER I

INTRODUCTION

1.1 MAX Phases and MAX-Metal Composites

It has always been of great importance to continuously advance our technology and the materials at our disposal. This chapter will focus on one group of materials that is incredibly fascinating in the world of material science and its subsidiaries. A very large reason that this group of materials has drawn the interests of scientists and engineers worldwide is their great resistance to many harmful forces. These materials have great resistance to oxidation and thermal shock, while keeping a high stiffness rating and machining very easily. The most incredible property of the materials is known as the kink band, this will be discussed in detail. This group of materials is known as MAX phases; the name arises from their chemistry and that will be discussed throughout the chapter. These materials are slowly working their way into the world as the technology advances; MAX phases are already replacing materials in industry from solid lubrication to structural applications.

During the mid-twentieth century, more than 100 new carbides and nitrides were discovered [1]. These were not intended to be discovered, and as many great new discoveries, were discovered by accident and it stirred up much confusion amongst the founders. These great confusions were left mostly unexplored because, at the time, the group that founded them had other projects going on and did not predict the immense properties that would be later discovered. It was not until almost thirty years later, in the

early 1990's, that these phases were revisited, this time with a drive to discover everything about them. The team, led by Dr. Barsoum in the Materials Engineering department at Drexel University, focused on the ternary compound Ti_2SiC_2 . This compound was successfully synthesized and fully characterized; with these results they realized they had unearthed a much larger and possibly ground-breaking new class of materials. These new phases of materials showed an incredible combination of ceramic and metallic properties [1]; it is as if the most favorable properties of each were present, replacing the limitations of each with the strengths of the other. The phases showed very high electrical and thermal conductivity, as if they were metallic, but also showed to be extremely resistant to oxidation and thermal shock, such as a ceramic would show. This discovery led to the formation of another pure phase material: Ti_2AlN_3 . When this material showed similar properties and had a very similar crystal structure, the team at Drexel University realized they were dealing with a much larger group of materials that would yield similar behavior and they began work on classifying them.

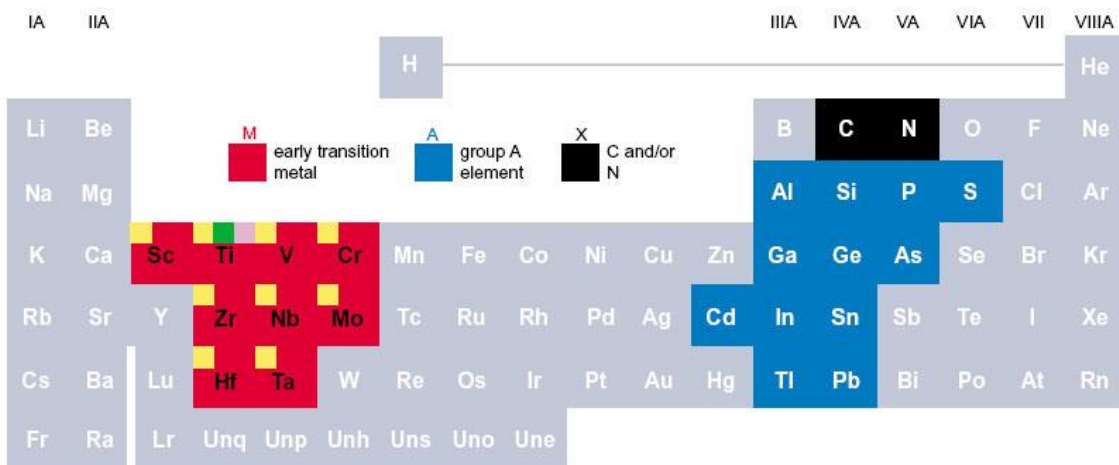


Figure 1.1. Periodic Table [2]

It turns out that with the general formula $M_{n+1}AX_n$, where $n=1,2$ or 3 , M is an early transition metal, A is an A-group element (mostly group IIIA or IVA), and X is either carbon or nitrogen; these properties are formed [1]. It's from this chemistry that the term "MAX phase" was originated, and a whole new area of materials research was formed. The main reason for the amount of attention that the MAX phases have received is their unique set of properties [1]. This can be explained using their atomic bonding and structural characteristics. They are similar to their corresponding binary carbides and nitrides in the fact of being elastically stiff, being great thermal and electrical conductors, having very high resistance to oxidation and other chemical attacks, and having relatively low thermal expansion coefficients [3]. With these properties being closely related to that of their binary structures, one would expect similar mechanical behaviors, but the MAX phases couldn't be more different in their mechanical properties. MAX phases are relatively soft (2-8 GPa) and are very machinable, resistant to thermal shock, and damage tolerant [3]. The MAX phases do vary amongst themselves and can be tuned to specific properties for the given application. Figure 1.2 shows the different variations of the unit cells when $n=1,2$ or 3 . At room temperature, MAX phases can have compressive strengths up to 1 GPa and fully recover upon load removal while dissipating 25% of the mechanical energy [4]. At higher temperatures, MAX phases undergo a brittle to plastic deformation and their corresponding mechanical behavior is a strong function of deformation rate [5]. It is the mechanical properties of the MAX phases that make them so distinct from other binary and ternary carbides [1, 5]. This article is set to gain an understanding of MAX phases and their properties, both elastic and mechanical, as well as formation processes and examples of several applications.

1.2 MAX Phase Unit Cell Variations

MAX phase unit cells are hexagonal $M_{n+1}AX_n$ with $n=1,2$ or 3 [1]. The variation in “ n ” is the main method of classifying the phases into three subgroups. There are approximately fifty M_2AX phases (or 211 phases) [6] and five M_3AX_2 (or 312 phases): Ti_3SiC_2 [7], Ti_3GeC_2 [8], Ti_3AlC_2 [9], Ti_3SnC_2 [10], and Ta_3AlC_2 [11]. The number of M_4AX_3 (or 413 phases) is growing since the discovery of the structure in Ti_3AlN_4 [12]. Latest discoveries of the 413 phases include the following: Ta_4AlC_3 [12], Nb_4AlC_3 [13]. The unit cells are illustrated below in Figure 1.2.

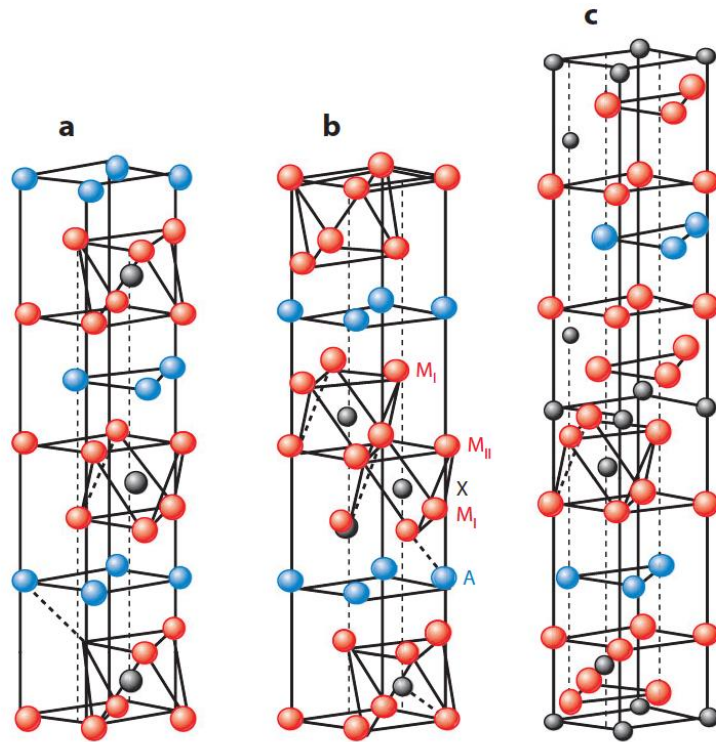


Figure 1.2. Illustrated variations of the MAX phases, where a, b, and c represent the unit cells for M_2AX (211), M_3AX_2 (312), and M_4AX_3 (413), respectively [1].

As stated above, the A-group elements that are most prevalent are groups IIIA and IVA, with the most versatile being aluminum. Aluminum forms nine compounds including

two nitrides, one 312 phase, and four 413 phases [5]. Gallium also forms nine compounds, however they are all 211 phases, six of which are carbides and three of them nitrides [5]. The 211 phases are by far the most prevalent MAX phases [1]. The unit cells of the MAX phases are characterized by the near close-packed M layers interleaved with layers of pure group A-element, with the X-atoms filling the octahedral sites between the former [1]. This is shown in Figure 1.2. The A-group elements are located at the centers of the trigonal prisms, which are slightly larger and can better accommodate the larger A-group atoms, as compared to the smaller octahedral sites [14].

Table 1.1 List of known MAX phases [2].

		A-group element				
		s^2 (group 12)	$s^2 p^1$ (group 13)	$s^2 p^2$ (group 14)	$s^2 p^3$ (group 15)	$s^2 p^4$ (group 16)
M element	211 Phases					
	3d	Ti ₂ CdC	Sc ₂ InC Ti ₂ AlC Ti ₂ GaC Ti ₂ InC Ti ₂ TiC V ₂ AlC V ₂ GaC Cr ₂ GaC Ti ₂ AlN Ti ₂ GaN Ti ₂ InN V ₂ GaN Cr ₂ GaN	Ti ₂ GeC Ti ₂ SnC Ti ₂ PbC V ₂ GeC Cr ₂ AlC Cr ₂ GeC	V ₂ PC V ₂ AsC	Ti ₂ SC
	4d		Zr ₂ InC Zr ₂ TiC Nb ₂ AlC Nb ₂ GaC Nb ₂ InC Mo ₂ GaC Zr ₂ InN Zr ₂ TiN	Zr ₂ SnC Zr ₂ PbC Nb ₂ SnC	Nb ₂ PC Nb ₂ AsC	Zr ₂ SC Nb ₂ SC
	5d		Hf ₂ InC Hf ₂ TiC Ta ₂ AlC Ta ₂ GaC	Hf ₂ SnC Hf ₂ PbC Hf ₂ SnN		Hf ₂ SC
	312 Phases					
	3d		Ti ₃ AlC ₂ V ₃ AlC ₂	Ti ₃ SiC ₂ Ti ₃ GeC ₂ Ti ₃ SnC ₂		
	5d		Ta ₃ AlC ₂			
	413 Phases					
	3d		Ti ₄ AlN ₃ V ₄ AlC ₃ Ti ₄ GaC ₃	Ti ₄ SiC ₃ Ti ₄ GeC ₃		
	4d		Nb ₄ AlC ₃			
5d		Ta ₄ AlC ₃				

Shown in Table 1.1 is the list of known MAX phases with their corresponding structures.

This list is incomplete as there is current research in this field and there may have been new discoveries since this report was compiled.

1.3 Elastic Properties of MAX Phases

As shown in Table 1.2, for the most part MAX phases are elastically stiff [5]. When this high stiffness rating is combined with the relatively low densities of some of the compounds (4-5 g/cm³), the specific stiffness of the MAX phases can be very high. It has been reported that Poisson's ratio for all MAX phases is approximately 0.2 [1], which is lower than the 0.3 value for titanium and is much closer to the 0.19 value of the near-stoichiometric TiC compound [5]. Possibly the most fascinating aspect of the MAX phases is their nonlinear elastic behavior. Unlike other elastically stiff materials, the MAX phases behave in a hysteretic manner [1]. Cyclic loading in compression or tension [4, 13] results in completely reversible hysteretic loops where the size and shape of the loop is strongly dependent on grain size [1]. When plotted on a stress vs. strain graph, MAX phases act very unlike their metallic or ceramic components in that they form what is known as a hysteresis loop during loading and unloading. The hysteresis loop behavior means that they experience opposite energy dissipation, thus causing no permanent plastic deformation. The hysteresis loop is caused by the formation of kink bands. A kink band is generally formed when a layered material is loaded parallel to its layers. For example, compressing a deck of cards along the layers will cause them to buckle and "kink". Kink band formation has been used to explain the deformation of numerous materials and structures; for example, organic crystals show kink band formation when deforming [14]. Due the common occurrence of kink bands in nature, there has been a great deal of research done studying them and their properties. This prior research made comparing the MAX phases kink bands a high priority in understanding more about the nature of the MAX phase.

Table 1.2. Density, shear modulus G , Young's modulus, E , and Poisson's ratio, ν , of select MAX phases [1].

Solid	Density (g cm^{-3})	G (GPa)	E (GPa)	ν
Ti_2AlC	4.1	118	277	0.19
$\text{Ti}_2\text{AlC}_{0.5}\text{N}_{0.5}$	4.2	123	290	0.18
V_2AlC	4.81	116	235	0.20
Cr_2AlC	5.24	102	245	0.20
	5.1	116	288	
Nb_2AlC	6.34	117	286	0.21
Ta_2AlC	11.46	121	292	
Ti_3SiC_2	4.52	139	343-339	0.20
Ti_3GeC_2	5.02	142	340-347	0.19
$\text{Ti}_3(\text{Si,Ge})\text{C}_2$	4.35	136.8	322	0.18
Ti_3AlC_2	4.2	124	297	0.20
Ti_3AlCN	4.5	137	330	0.21
Cr_2GeC	6.88	80	245	0.29
V_2GeC				
Ti_2SC		125	290	0.16
Ti_2SnC				
Nb_2SnC			216	
Zr_2SnC			178	
Hf_2SnC			237	
Nb_2AsC	8.05			
Nb_4AlC_3	6.98	127	306	
$\beta\text{-Ta}_4\text{AlC}_3$	13.2	132	324	
Ti_4AlN_3	4.7	127	310	0.22
$\text{TiC}_{0.96}$	4.93	205	≈ 500	0.19
Zr_2SC	6.20			

1.4 Machinability and Mechanical Behavior of MAX Phases

MAX phases are, for lack of a better term, a hybrid of ceramics and metals. Much like ceramics, the MAX phases will decompose when exposed to temperatures over 1,800-2,000 °C, whereas this temperature would melt just about all metals. MAX phases with their relatively low density, high stiffness and resistance to oxidation are very similar to that of a typical ceramic. Ceramics can be very difficult to machine due to their high stiffness and brittleness. This is where the metallic properties of the MAX

phase come into effect. The machinability rating of the MAX phases is one of the biggest selling points; MAX phases are easily machined with tools as basic as a hand drill or hacksaw. The layered nature of the MAX phases and their slip systems allow this to be possible [3]. With the metallic properties mixed with the ceramic, a MAX phase becomes a layered solid, such as mica, ice, or graphite [1]. Mica, ice, and graphite all lack the five independent slip systems needed for ductility, this causes large internal stresses and uneven stress states when loaded. These slip systems, or lack thereof, are another important consequence of kink band formation. One of the most important factors of understanding what is going on at high temperatures of the MAX phase is that in contrast to almost all other crystalline solids, the fracture toughness, K_{Ic} , decreases above the transition temperature [3]. The hardness of the MAX phase is very interesting; MAX phases are relatively soft and very damage tolerant. The hardness is dependent of the load. As the applied load grows larger, the hardness of the MAX phase increases [1]. MAX phases are quite damage tolerant, as shown Figure 1.3, a MAX phase solid was struck numerous times with a hammer while showing indentations. The indentations in the figure are not unlike ones observed performing the same test on a metal.



Figure 1.3. Picture of MAX phase Ti_2AlC after hit with a steel hammer; picture's width is about 20cm. Picture courtesy of 3-ONE-2.

It would be impossible to include all of the amazing and unusual properties of the MAX phases into a short summary; this paper was meant to inform the reader about this new phase of materials that is being created. Key properties of the MAX phases were included to highlight a few of the more unusual aspects regarding the MAX phases and how fascinating they are. There are hundreds of scientific journals explaining each component of this report in detail if the reader is requesting further information or explanation.

1.5 MAX Phase-Metal Composites

Composites of MAX phases with metals (MAXMET) are highly regarded from both a fundamental and an applied perspective. Zhang et al. [15] proposed Ti_3SiC_2-Cu as a new electro-friction composite material. Gupta et al. [14, 16] developed composites consisting of MAX phases and Ag, which showed solid lubrication over a wide range of

temperatures. Anasori et al. [17] reported MAX phase composites with up to 80 vol% Mg are readily machinable, relatively stiff, strong, light, and exhibit ultrahigh damping. Increasing the Mg volume fraction leads to lighter composites with higher damping characteristics at lower stresses. Wang et al. [18] fabricated Al-matrix MAXMETs from pure Al and 40 vol% Ti_3AlC_2 powders using a hot isostatic pressing technique. The yield strength of the Al- Ti_3AlC_2 composite was found to be twice that of pure Al [18]. Hu et al. [19] reported that the specific strength of an Al- Ti_2AlC alloy composite was 50% higher than that of peak-aged Al alloy in an interpenetrating 40 vol% - aluminum alloy composite [19]. However, the authors did not investigate the entire spectrum of Al-MAX composites. There is a huge potential for multifunctional materials that can be developed using MAX phases as a constituent in Metal Matrix Composites (MMCs) or Ceramic Matrix Composites (CMCs). Although it is well known that Al and Al alloys have poor tribological behavior [21], Al-based MMCs reinforced with rigid ceramic particulates have high specific strength and modulus, good wear resistance, and are easily machinable [22, 23]. They have become increasingly important for structural applications in aerospace, automotive and other transport industries. Due to the incorporation of hard ceramic particles, the machining of MMCs is difficult, and complex tools are necessary to machine them [24-26]. It is expected that the addition of MAX phases will further enhance the mechanical behavior and machinability of MMCs. The novel MMCs will also have multifunctional attributes, for example, enhanced damping, hardness, and tribological behavior. For rapid usage and fabrication of Al-MAX composites, novel manufacturing methods should be explored. In this paper, we report for the first time the

tribology characterization for novel Al-matrix composites reinforced with Ti_3SiC_2 particulates (nanolaminates).

1.6 MAX Phase-Epoxy Composites

It has previously been explained that MAXMETs play a significant role from both a fundamental and an applied perspective. Gupta et al. [14-21] have comprehensively studied the tribology of MAX phases and their composites. As a part of his previous study, the authors demonstrated that MAX Phase-based composites can be used as shafts against Superalloy (SA) foils for different foil bearing applications at 50,000 rpm from RT up to 550°C during thermal cycling [20]. Earlier, despite several years of research, there were no structural materials which could be used as a solid lubricant in temperatures ranging from RT to 550°C [21, 22]. Thus, there is a huge potential for materials that can be used in different tribological and engineering systems, e.g., air-foil bearings, gas turbine seals, cylinder wall/piston ring lubrication for low-heat rejection diesel engines, various furnace components, among many others [14]. By manufacturing composites with hexagonal metals, it is also possible to enhance the damping behavior of these materials [23-25]. Recently, Ansari et al. [25] fabricated readily machinable, relatively stiff, strong and light MAX-Mg composites with ultra-high damping, where ~30% of the mechanical energy is dissipated at 250 MPa.

Polymers and their composites are currently used extensively in aerospace, automobile, and chemical sectors due to their low density, excellent strength to weight ratios, resistance to corrosion, self-lubricating properties, low coefficient of friction (μ) and better wear resistance, and in some cases, provide an alternative to metallic materials [26-34]. Generally, ceramic particles are added to a polymer matrix to enhance the

mechanical and tribological performance [28-31]. Unfortunately, there has been no exploratory research on the design of MAX-Polymer (MAXPOL) composites. Here, in Chapter 4, we report for the first time the synthesis and characterization of Epoxy- Ti_3SiC_2 composites.

CHAPTER II

SYNTHESIS OF NOVEL MAX-AL(ALUMINUM) COMPOSITES

2.1 Fabrication Processes

Ti_3SiC_2 powder (Kanthal, Hallstahammar, Sweden) and the tailored concentrations of Al Powder (-325 mesh, Alfa Aesar, Ward Hill, MA) was dry ball milled (8000 M mixer Mill, SPEX SamplePrep, Metuchen, NJ) in batches of 1 cubic centimeter with polymethyl methacrylate (PMMA) (2 spheres, 0.537 g each) for 2 minutes. The mixed powders were then cold pressed in a ~12.7 mm die with a uniaxial compressive stress ~210 MPa. Novel Al-matrix composites were designed with 35 vol% Ti_3SiC_2 (Al(65)- Ti_3SiC_2 (35)), 20 vol% Ti_3SiC_2 (Al(80)- Ti_3SiC_2 (20)), 10 vol% Ti_3SiC_2 (Al(90)- Ti_3SiC_2 (10)), and 5 vol % Ti_3SiC_2 (Al(95)- Ti_3SiC_2 (5)) in an Al matrix. For comparison, pure Al samples were also prepared under similar conditions. Al(65)- Ti_3SiC_2 (35) samples were fabricated by heating the samples at 10°C/min to 760° C, and then isothermal holding at 760°C for 30 min. All the other compositions were manufactured by heating the samples at 10°C/min to 700°C, and then isothermal holding at 700°C for 5 minutes.

Samples were coated with Au/Pd, using a Balzers SCD 030 sputter coater (BAL-TEC RMC, Tucson AZ USA), and then secured on aluminum mounts. Secondary Electron (SE) and Backscattered Electron (BSE) images were obtained using a JEOL JSM-

6490LV Scanning Electron Microscope (JEOL USA, Inc., Peabody, Massachusetts). X-ray information was obtained via Thermo Nanotrace Energy Dispersive X-ray detector with NSS-300e acquisition engine. It is important to note at this juncture that the accuracy of measuring carbon is quite low in the EDS. It follows that implicitly, and unless otherwise noted, the compositions listed could very well contain C. This is especially true of sub-stoichiometric oxides. In addition, the chemistry of a region that was deemed chemically uniform at the micron level as quantified by Energy Dispersive Spectroscopy (EDS) – is designated with two asterisks, as *microconstituent* to emphasize that these areas are not necessarily single phases. The presence of C in these tribofilms is shown by adding {C_x} in the composition [14]. For observing the grains, each sample was etched with Kelly's Reagent for 15 s and then rinsed with water.

XRD measurements were performed on an AXS D8 Bruker X-ray Diffraction System, an x-ray diffractometer equipped with a two-dimensional Hi-Star area detector, video camera / laser alignment system, and a Cu x-ray radiation point source.

2.2 Results and Discussion

Figure 2.1 shows the XRD profile of all the different compositions. In the XRD profile of Al(65)- Ti₃SiC₂ (35) - Ti₃SiC₂, Al phases, TiC and Al₃Ti phases were detected. All the other compositions showed significantly small or negligible amount of Al₃Ti and TiC phases which indicates that there was mild or negligible reaction in these compositions. As mentioned earlier, Al(65)- Ti₃SiC₂ (35) composition was fabricated at 760°C for 30 min, whereas all the other compositions were fabricated at 700°C for 5 min. Thus, the higher temperature during processing is responsible greater reaction in the Al(65)- Ti₃SiC₂ (35) .

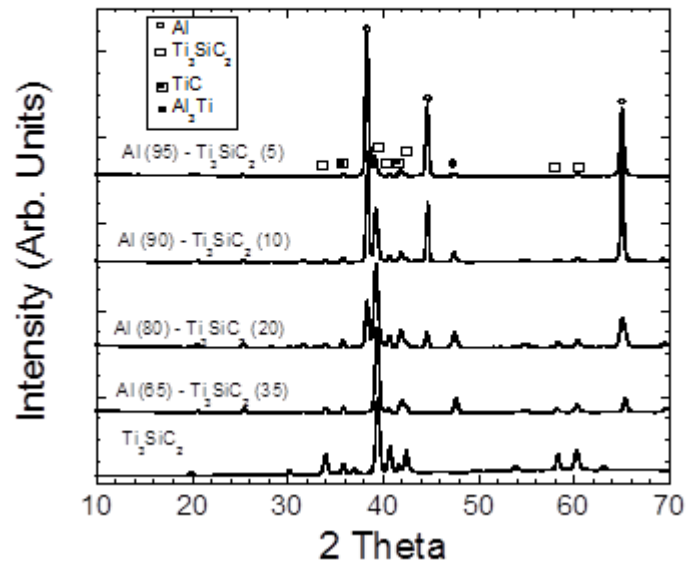


Figure 2.1. XRD profiles of different composites of Al-Ti₃SiC₂.

During the optimization studies, despite several attempts, Al(65)- Ti₃SiC₂ (35) could not be sintered at lower temperatures. Thus, for fabricating Al- Ti₃SiC₂ with higher concentrations of Ti₃SiC₂ (>35 vol%) alternative methods of fabrication like Hot Pressing (HP), or Hot Isostatic Press (HIP) should be explored.

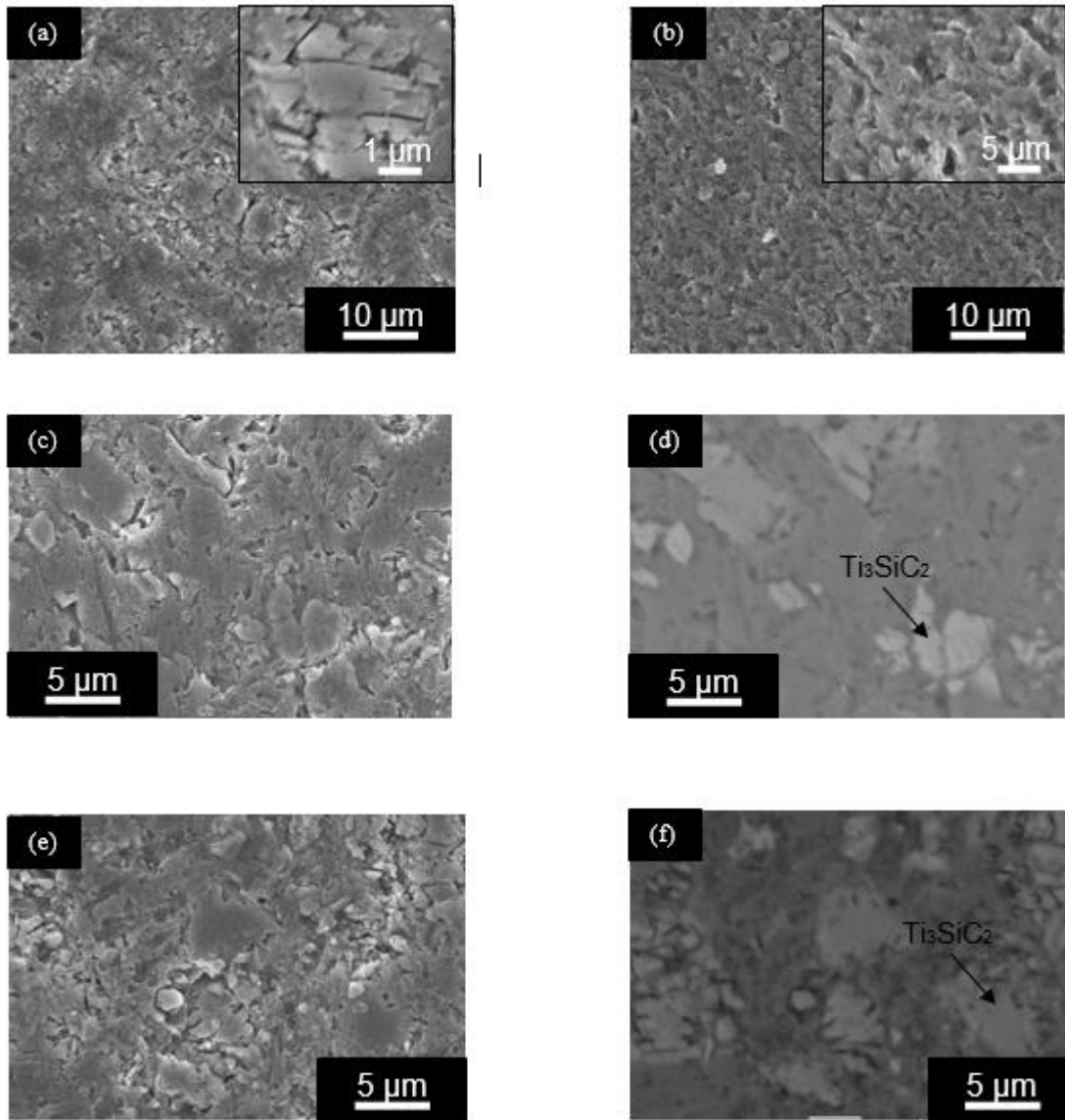


Figure 2.2. Secondary Electron SEM micrographs of etched surfaces of sintered, (a) Al, (b) 5 vol% Ti_3SiC_2 , (c) 10 vol% Ti_3SiC_2 and (d) Backscattered (BSE) image of the same region, (e) 20 vol% Ti_3SiC_2 , and (f) BSE image of the same region, in Al matrix (Al- Ti_3SiC_2 composites).

Figure 2.2 shows the SE and BSE SEM images of the etched surface of Al-MAX phase composites. In all the composites, Ti_3SiC_2 particles are well-dispersed in the matrix. The grain size of all the compositions was similar and varied between 2-10 μm .

Figure 2.3a1 shows the SEM image of the polished surfaces of Al(80)- Ti₃SiC₂ (20) composite. Figures 2.3 shows the SE and BSE image of a Ti₃SiC₂ particle embedded in it. No significant interfacial reaction was observed in the microstructure.

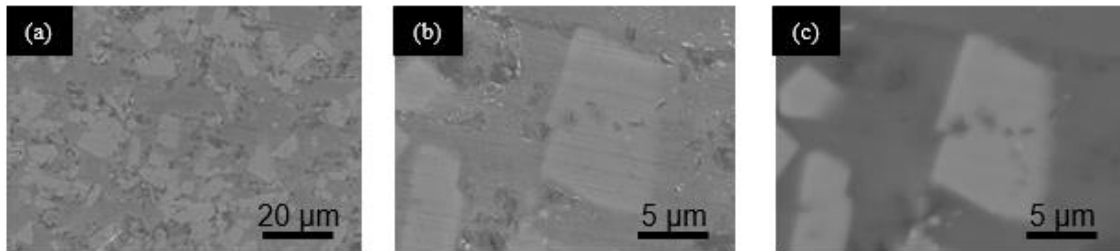


Figure 2.3. Secondary Electron images of Al(80)-Ti₃SiC₂(20) composites at, (a) low, and (b) higher magnification and (c) BSE image of the higher magnification region.

Figure 2.4a shows the change in porosity as a function of processing temperatures. The porosity changed linearly with the composition. This result shows that the processing of Al-matrix composites by liquid phase sintering becomes difficult as the concentration of Ti₃SiC₂ in the Al matrix increases. Figure 2.4b shows the compressive strength versus displacement profiles of all the Al matrix compositions. All the compositions, except Al(65)-Ti₃SiC₂(35), showed gradual failure. The Al(65)-Ti₃SiC₂(35) composition showed brittle failure. Figure 2.4c shows the comparison of yield strength and hardness of these composites.

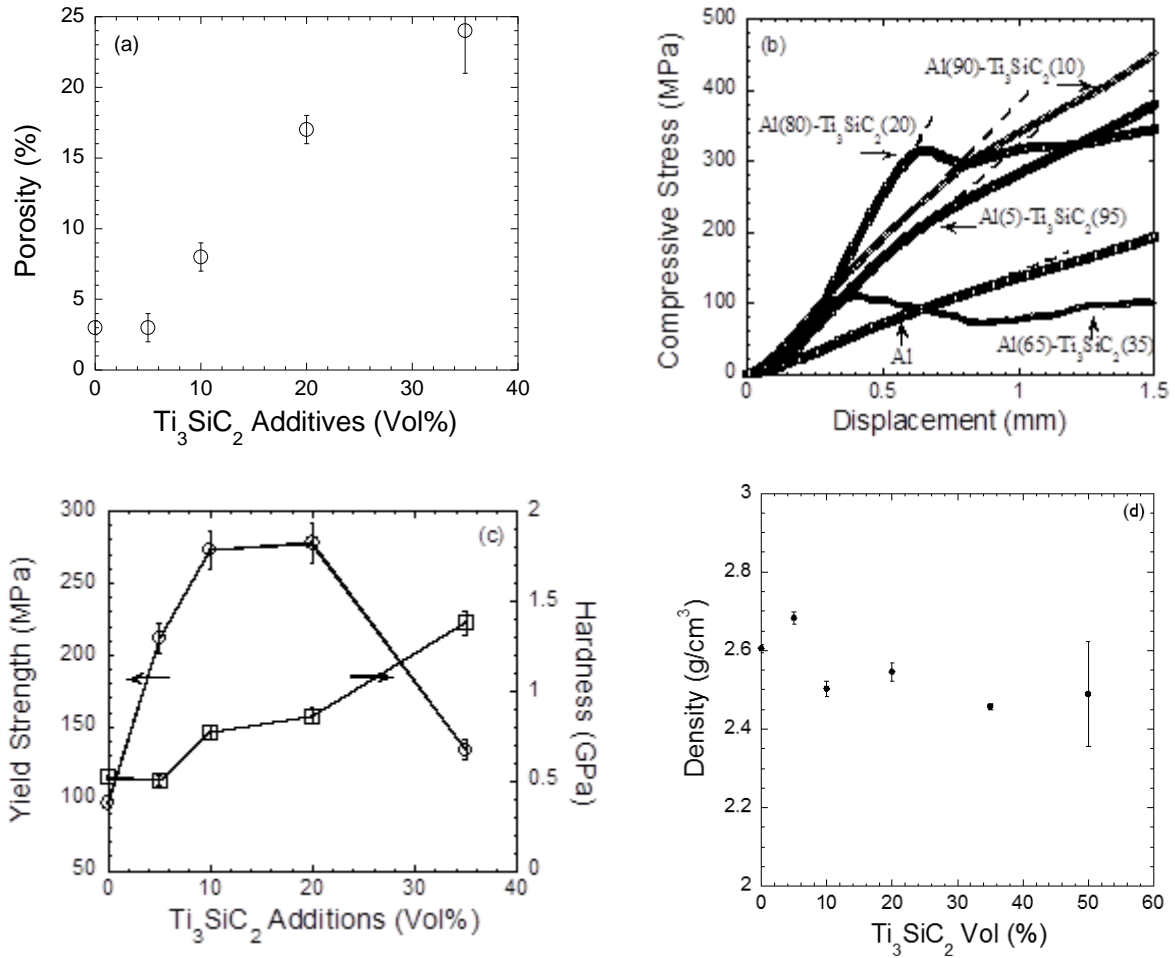


Figure 2.4. Plots of Al-Matrix properties, (a) change in porosity versus different vol% of Ti_3SiC_2 additions in the Al matrix, (b) compressive stress versus displacement profiles of different Al matrix composites, and (c) the effect of Ti_3SiC_2 additions on the yield strength (Y1 axis) and hardness (Y2 axis) of Al matrix composites, (d) actual densities of the composites.

The Al had a compressive strength of 97 ± 6 MPa. When the volume fraction of Ti_3SiC_2 increased to 5 vol% and 10 vol% in the composites, the compressive strength increased significantly to 212 ± 27 MPa, and 273 ± 52 MPa, respectively. As the volume fraction of Ti_3SiC_2 was further increased to 20 vol%, the compressive strength mildly increased to 278 ± 48 MPa. However, in Al(65)- Ti_3SiC_2 (35), the compressive strength decreased to 134 ± 20 MPa. The hardness of the samples increased linearly as a function of Ti_3SiC_2 content. These results conclusively show that the addition of Ti_3SiC_2 particles remarkably improves the compressive strength and hardness of the Al matrix composites. The lower strength of Al(65)- Ti_3SiC_2 (35) samples can be explained due to the higher porosity of these composites (Fig2.4a). It is possible the presence of Ti_3SiC_2 particles at the phase boundaries can cause the enhancement of mechanical strength. Further investigations are needed to understand the definite mechanisms for the enhancement in mechanical strength.

2.3 Conclusions

Reported for the first time is the synthesis and fabrication of Ti_3SiC_2 reinforced Al-matrix composites by pressureless sintering. The addition of Ti_3SiC_2 enhanced the mechanical and tribological performance of the Al-matrix composites.

CHAPTER III

SYNTHESIS OF NOVEL MAX-Sn(TIN) COMPOSITES

3.1 Fabrication Process

Ti_3SiC_2 powder (Kanthal, Hallstahammar, Sweden) and calculated concentrations of Sn Powder (-100 mesh, Alfa Aesar, Ward Hill, MA) were dry ball milled (8000 M mixer Mill, SPEX SamplePrep, Metuchen, NJ) in batches of 1 cubic centimeter with polymethyl methacrylate (PMMA) (2 spheres, 0.537 g each) for 2 minutes. All compositions were then sintered in atmospheric air using hot pressing (MTI Corporation, EQ-HP-6T, Richmond, CA) (HP) in a ~25.4 mm die at a uniaxial compressive stress of ~112 MPa and a temperature of 240°C for 5 minutes. Composites were allowed to cool in the HP to room temperature (RT) before characterization. Novel Sn-matrix composites were designed by adding 30 vol% (Sn(70)- Ti_3SiC_2 (30)), 20 vol% (Sn(80)- Ti_3SiC_2 (20)), 10 vol% (Sn(90)- Ti_3SiC_2 (10)), 5 vol% (Sn(95)- Ti_3SiC_2 (5)) Ti_3SiC_2 in the Sn matrix. For comparison, pure Sn was fabricated using the same method.

The composites were then machined into ~3 mm cubes for characterization of the mechanical behavior. Compression testing was conducted in a Shimadzu AG-IS UTM (Shimadzu AD-IS UTM, Shimadzu Scientific Instruments Inc., Columbia, MD). For each composition, a set of 3 samples were tested at a deflection rate of 1mm/min.

Experimental limitations did not allow for accurate measurement of the actual strain in each composite, stress verse displacement plots are reported. Yield strength is defined as the critical stress at which the stress verse displacement plot transitions from the linear to

non-linear regime. The linear region of the composites had a regression fitting of $R^2 > 0.95$. Reported within this text is the average of 3 yield strength measurements for each composite. Prior to hardness testing all composites were polished ($R_a < 1\ \mu\text{m}$) and then tested on a Vicker's micro-hardness indenter (Mitutoyo HM-112, Mitutoyo Corporation, Aurora, IL). Vicker's hardness was measured by loading the samples at 9.8 N for 15 s. An average of five readings for each composite was measured and is reported in this text.

Samples were coated with Au/Pd by using a Balzers SCD 030 sputter coater (BAL-TEC RMC, Tucson AZ USA), and then mounted on aluminum mounts. Secondary electron (SE) and Backscattered Electrons (BSE) images were obtained using a JEOL JSM-6490LV Scanning Electron Microscope (JEOL USA, Inc., Peabody, Massachusetts.) X-ray information was obtained via a Thermo Nanotrace Energy Dispersive X-ray detector with NSS-300e acquisition engine. It is important to note at this juncture that the accuracy of measuring C is quite low in the EDS. It follows that implicitly, and unless otherwise noted, the compositions listed could very well contain C. This is especially true of sub-stoichiometric oxides. In addition, the chemistry of a region that was deemed chemically uniform at the micron level as quantified by Energy Dispersive Spectroscopy (EDS) – is designated with two asterisks, as *microconstituent* to emphasize that these areas are not necessarily single phases. The presence of C in these tribofilms is shown by adding $\{C_x\}$ in the composition [14].

XRD measurements were performed on a Bruker Microdiffractometer, an x-ray diffractometer equipped with a two-dimensional Hi-Star area detector, video camera / laser alignment system, and a Cu x-ray radiation point source. Generated x-rays were conditioned with an incident beam graphite monochromator (Cu K_α pass-through

filter) and collimated with a 0.8 mm collimator. The microdiffractometer sample stage was equipped with a $\frac{1}{4}$ circle Eulerian cradle which allows for three sample rotation angles: ω – incident x-ray angle of incidence (co-linear tilt), χ – sample tilt (out-plane tilt), and φ – in-plane rotation.

3.2 Results and Discussion

Figure 3.1 is the phase analysis of all composites of Sn and Ti_3SiC_2 . As noted in the introduction, all composites were sintered at a low temperature of 240°C for 5 minutes by hot pressing. At this low temperature, it was expected that no or little reaction between the Sn and Ti_3SiC_2 particulates and this is proved to be true as shown in figure 3.1

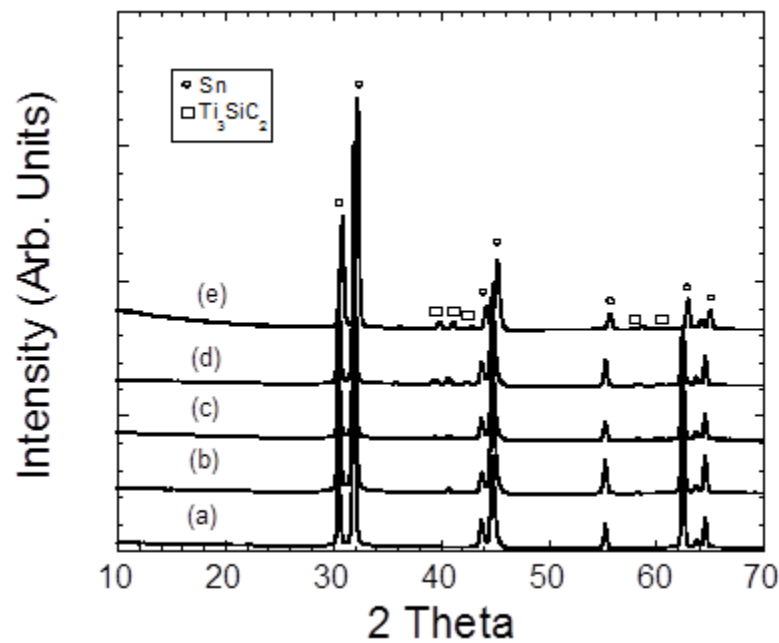


Figure 3.1. XRD profiles of, (a) Sn, (b) Sn(95)- Ti_3SiC_2 (5), (c) Sn(90)- Ti_3SiC_2 (10), (d) Sn(80)- Ti_3SiC_2 (20), (e) Sn(70)- Ti_3SiC_2 (30).

Figure 3.2 shows Secondary Electron (SE) SEM of Sn-matrix composites, in all composites the Ti_3SiC_2 particles are well-dispersed in the Sn matrix.

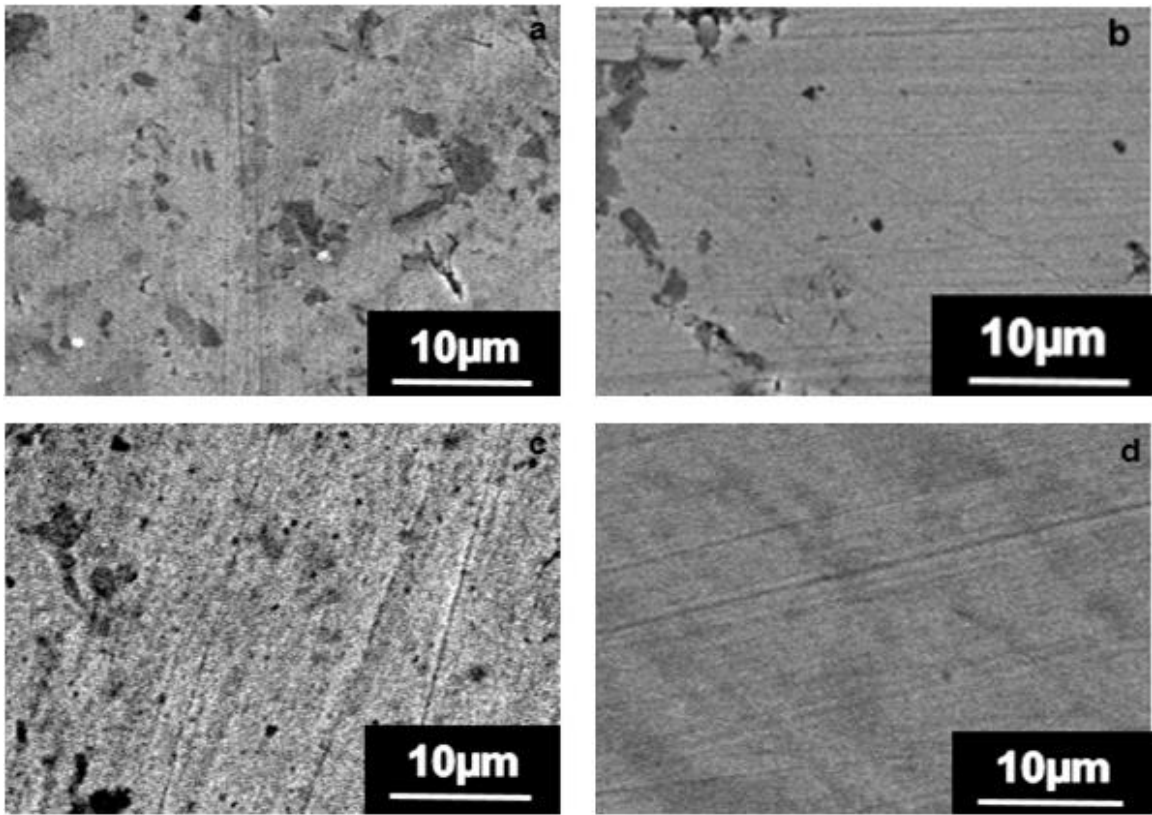


Figure 3.2. SE SEM of (a) Sn(70)- Ti_3SiC_2 (30), (b) Sn(80)- Ti_3SiC_2 (20), (c) Sn(90)- Ti_3SiC_2 (10), (d) Sn(100)

Figure 3.3 shows the porosity of the composites as a function of Ti_3SiC_2 additions. The addition of greater concentrations of Ti_3SiC_2 shows a near linear relationship with increased porosity in the composites. The results show that with increased Ti_3SiC_2

concentrations in the Sn matrix, it becomes difficult to make dense samples via hot pressing and other methods of fabrication are required.

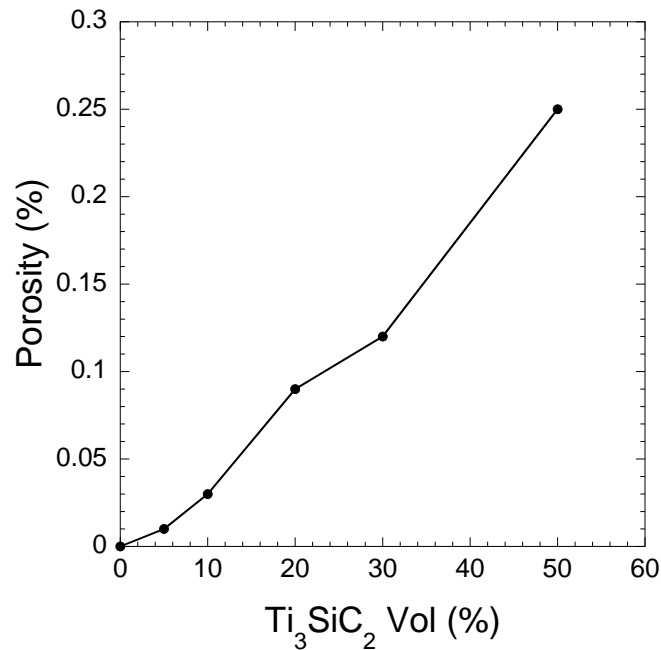


Figure 3.3. Porosity change with the increase of Ti₃SiC₂ vol%.

Figure 3.4a shows the compressive strength profiles plotted against displacement in the Sn-matrix composites. All compositions, except for Sn(70)- Ti₃SiC₂ (30), showed gradual failure. Brittle failure was observed in Sn(70)- Ti₃SiC₂ (30). Figure 3.4b was plotted to show a direct comparison of the yield strength and the hardness of the composites. Pure Sn had a compressive yield strength of 47 ± 3 MPa, when 5 vol% and 10 vol% Ti₃SiC₂ was dispersed into the Sn matrix, the compressive yield strength was increased to 57 ± 4 MPa and 58 ± 3 MPa, respectively.

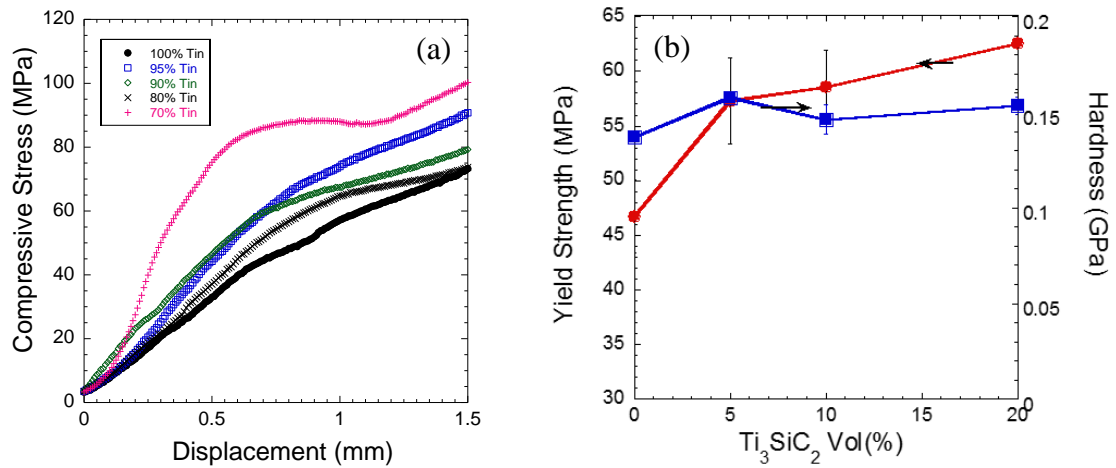


Figure 3.4. Compressive strength profiles of Sn-matrix composites (a) and comparison of compressive strength to the hardness of the composites (b).

As the volume fraction of Ti_3SiC_2 was further increased to 20 vol%, a slight increase was observed in the compressive yield strength to 63 ± 4 MPa. When the volume fraction of Ti_3SiC_2 was increased to 30 vol% in the Sn matrix, the compressive strength was further increased to 75 ± 14 MPa where brittle failure was observed. It is important to note that the higher deviation in the strength of the Sn(70)- Ti_3SiC_2 (30) composite can be attributed to the non-uniform porosity throughout the composite. The hardness of the composites is relatively unchanged as the volume fraction of Ti_3SiC_2 is increased up to 30 vol%. The results suggest that the addition of Ti_3SiC_2 particulates in a Sn matrix can increase the compressive strength of the Sn matrix while the hardness remains relatively unchanged and the actual density of the composites is decreasing with the addition of Ti_3SiC_2 .

3.3 Conclusions

In this thesis, we report for the first time, the synthesis of novel Sn-matrix composites with Ti_3SiC_2 particulates well-dispersed in the matrix. The addition of Ti_3SiC_2 particulates into the matrix greatly increased the compressive strength of the matrix, while reducing the overall density of the composite and leaving the hardness relatively unchanged.

CHAPTER IV

SYNTHESIS OF NOVEL MAX-EPOXY COMPOSITES

4.1 Fabrication Processes

During this study three different compositions of epoxy matrix reinforced composites with 20.7 vol% (epoxy(20.7)- Ti_3SiC_2 (79.3)), 32.6 vol% (epoxy(32.6)- Ti_3SiC_2 (67.4)), and 71.6 vol% (epoxy(71.6)- Ti_3SiC_2 (28.4)) were fabricated. For comparison, a pure epoxy sample was also prepared under similar conditions.

The base epoxy samples were fabricated by mixing ~0.9 g hardener (West System 206 Slow Hardener, Gougen Brothers, Inc. Bay City, MI) and ~4.5 g epoxy resin (West System 105 Epoxy Resin, Gougen Brothers, Inc. Bay City, MI) with a wooden spatula by hand, stirring for ~1 min. Thereafter, the composition was cast in ~25 mm plastic molds. All the compositions were fabricated by mixing the Ti_3SiC_2 powders (-325, Kanthal, Hallstahammar, Sweden) with the epoxy composition as described above. The final fabrication process was different for the composite samples.

The epoxy(20.7)- Ti_3SiC_2 (79.3) composition was cast by following the method described above. Both the epoxy(32.6)- Ti_3SiC_2 (67.4) and epoxy(71.6)- Ti_3SiC_2 (28.4) compositions were too viscous to be manually cast. The epoxy(32.6)- Ti_3SiC_2 (67.4) composition was cast in ~25 mm molds by applying vibration during casting. The epoxy(71.6)- Ti_3SiC_2 (28.4) composite was fabricated by cold pressing the mixture in ~12.5 mm dies while applying an uniaxial stress of ~105 MPa. The relative volume

fraction of polymer in the epoxy(71.6)-Ti₃SiC₂(28.4) composite was accurately determined by baking the composite in a tube furnace at 400°C for 4 h in an inert Ar environment. The weight analysis showed that the composites have ~71.6 vol% Ti₃SiC₂. All compositions were cured for 24 h under ambient conditions.

Samples were secured to aluminum mounts and coated with gold/palladium using a Balzers SCD 030 sputter coater (BAL-TEC RMC, Tucson AZ). SE and BSE Images were obtained by using a JEOL JSM-6490LV Scanning Electron Microscope (JEOL USA, Inc., Peabody, Massachusetts). X-ray information was obtained via a Thermo Nanotrace Energy Dispersive X-ray detector with NSS-300e acquisition. It is important to note at this juncture that the accuracy of measuring Carbon is quite low in the EDS. It follows that implicitly, and unless otherwise noted, the compositions listed could very well contain C. This is especially true of sub-stoichiometric oxides. In addition, the chemistry of a region that was deemed chemically uniform at the micron level as quantified by Energy Dispersive Spectroscopy (EDS) – is designated with two asterisks, as *microconstituent* to emphasize that these areas are not necessarily single phases. The presence of C in these tribofilms is shown by adding {C_x} in the composition [14].

4.2 Results and Discussion

Figure 4.1 shows the microstructure of the epoxy-32.6 vol% Ti₃SiC₂ (Figs. 1a-b) and epoxy -71.6 vol% Ti₃SiC₂ (Figs. 1c-d) composites. By examining the microstructures, we can conclude that Ti₃SiC₂ particles are well-dispersed in the epoxy matrix. Figure 2a shows the plot of compressive strength versus displacement of the as synthesized composites. The increase in the concentration of Ti₃SiC₂ in the epoxy enhanced the stiffness of the composites.

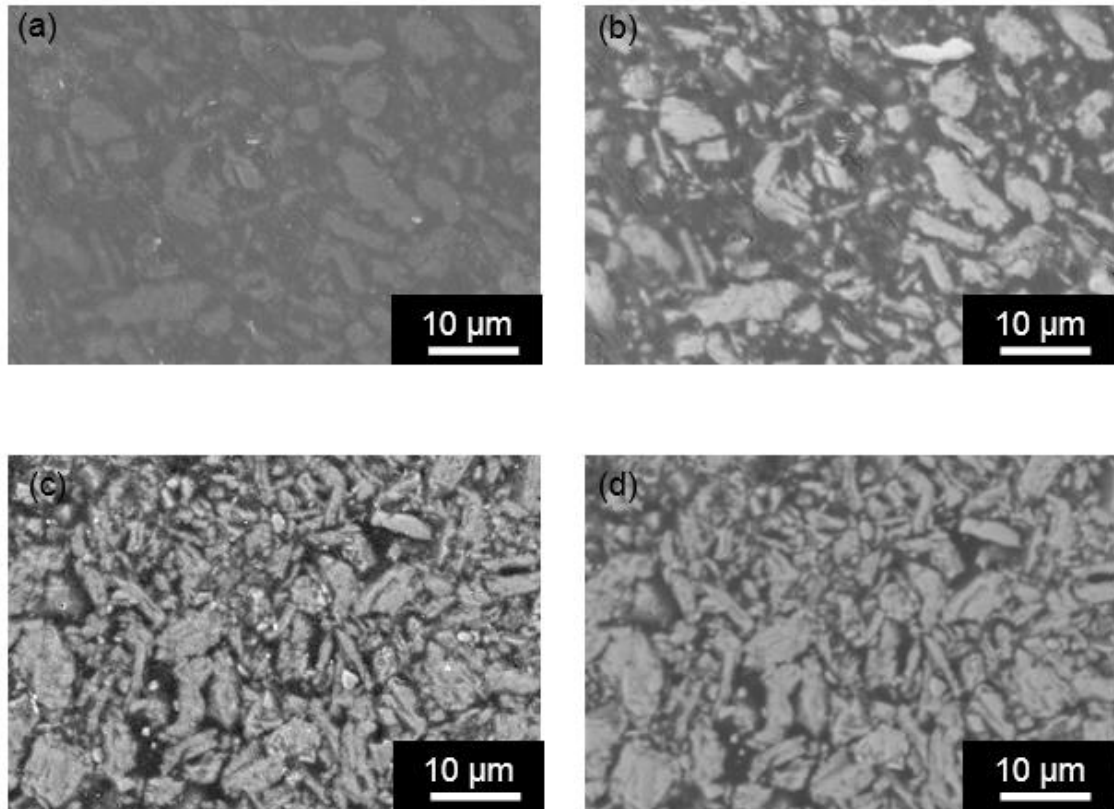


Figure 4.1. SEM micrographs of epoxy-matrix composites, (a) epoxy-32.6 vol% Ti₃SiC₂ in SE mode, (b) BSE image of the same region, and (c) epoxy-71.6 vol% Ti₃SiC₂ in SE mode, and (d) BSE image of the same region.

All the compositions displayed gradual failure. Figure 4.2b plots the UCS (Y1 axis) and the hardness (Y2 axis) versus the concentration of the Ti₃SiC₂ additives. The UCS gradually increased from 88.8 ± 4.74 MPa in epoxy to 124 ± 4.57 MPa in epoxy-32.6 vol% Ti₃SiC₂, thereafter the UCS dropped slightly to 118 ± 8.06 MPa in epoxy-71.6 vol% Ti₃SiC₂ composites. It is not clear what causes the strength decrease of epoxy-71.6 vol% Ti₃SiC₂ as compared to epoxy-32.6 vol% Ti₃SiC₂. Most probably, the grain boundary decohesion of Ti₃SiC₂-polymer interface can cause the lower strength of the samples with higher concentration of Ti₃SiC₂. In the future, the mechanical behavior of different types of

MAXPOL composites should be explored in detail. The hardness gradually increased from 189 ± 6 MPa in epoxy to 288 ± 3 MPa in epoxy-32.6 vol% Ti_3SiC_2 and 518 ± 13 MPa in Epoxy-71.6 vol% Ti_3SiC_2 , respectively. Figure 4.1 shows the microstructure of the epoxy-32.6 vol% Ti_3SiC_2 (Figs. 1a-b) and epoxy-71.6 vol% Ti_3SiC_2 (Figs. 1c-d) composites. By examining the microstructures, we can conclude that Ti_3SiC_2 particles are well dispersed in the epoxy matrix.

Figure 4.2a shows the plot of compressive strength versus displacement of the as synthesized composites. The increase in the concentration of Ti_3SiC_2 in the epoxy enhanced the stiffness of the composites. All the compositions displayed gradual failure. Figure 4.2b plots the UCS (Y1 axis) and the hardness (Y2 axis) versus the concentration of the Ti_3SiC_2 additives.

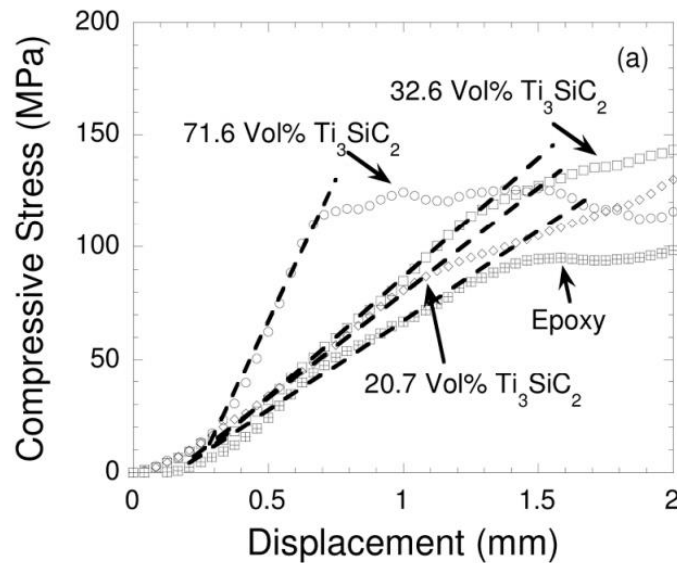


Figure 4.2a. Plot of compressive strength versus displacement.

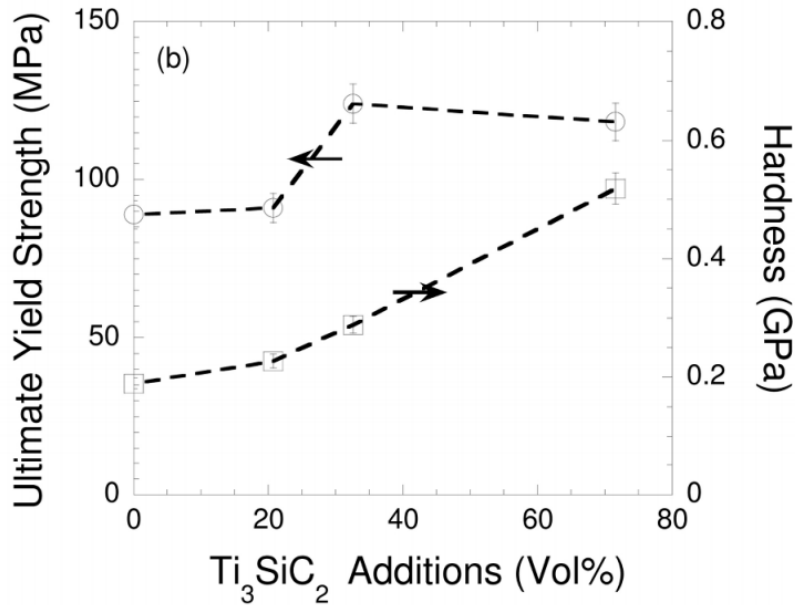


Figure 4.2b. Ultimate Yield Strength (UYS) (Y1 axis) and hardness (Y2 axis) versus different volume fraction additions of Ti_3SiC_2 in the epoxy matrix.

4.3 Conclusions

We synthesized the epoxy- Ti_3SiC_2 composites for the first time. The microstructure analysis showed that Ti_3SiC_2 phase is well-dispersed in the epoxy matrix. The microstructure evaluation by SEM (Scanning Electron Microscopy) showed that Ti_3SiC_2 particles are well dispersed in the epoxy matrix. The UCS (Ultimate Compressive Strength) increased from 88.8 ± 4.74 MPa in epoxy to 124 ± 4.57 MPa in epoxy-32.6 vol% Ti_3SiC_2 , thereafter the UCS dropped slightly to 118 ± 8.06 MPa in epoxy-71.6 vol% Ti_3SiC_2 . The hardness gradually increased from 189 ± 6 MPa in epoxy to 288 ± 3 MPa in epoxy-32.6 vol% Ti_3SiC_2 and 518 ± 13 MPa in epoxy-71.6 vol% Ti_3SiC_2 as the concentration of the Ti_3SiC_2 was systematically increased in the epoxy matrix.

CHAPTER V

FUTURE STUDIES

5.1 Synthesis of Novel MAX-Al(Aluminum)-Sn(Tin) Composites

Throughout this research there has been a common theme of attempting to increase the relative density of the novel composites that have been fabricated in Chapters 2-4. In Chapter two, it was demonstrated that a metal matrix with MAX phase particulates can have excellent mechanical properties when fabricated using pressureless, liquid phase sintering. The limitation with liquid phase sintering is the uncontrollable volatilization of alloying elements that have a melting temperature that is lower than what is required for sintering. This volatilization leaves pores in the material, and making dense samples becomes impossible. It is known that low-Sn, Al-based alloys where $\text{Sn} < 7\%$, with the addition of low amounts of strengthening elements such as copper(Cu) or nickel(Ni) are used for connecting rods and thrust bearings in high duty engines. Al-Sn alloys have an excellent compromise of high fatigue strength and good surface properties and when used with a hardened steel crankshaft, it allows for significantly higher loading than in Sn-Pb(lead) bearings. In Chapter three, a lower melting temperature metal, Sn, was used for the metal matrix by hot pressing for the fabrication method. The samples made by hot pressing had much higher relative densities than the composites that were fabricated by liquid phase sintering.

5.2 Manufacturing Details

Ti₃SiC₂ powder (Kanthal, Hallstahammar, Sweden) and calculated concentrations of Al Powder (-325 mesh, Alfa Aesar, Ward Hill, MA) and Sn Powder (-100 mesh, Alfa Aesar, Ward Hill, MA) were dry ball milled (8000 M mixer Mill, SPEX SamplePrep, Metuchen, NJ) in batches of 1 cubic centimeter with polymethyl methacrylate (PMMA) (2 spheres, 0.537 g each) for 2 minutes. All the compositions were then sintered in atmospheric air using hot pressing (MTI Corporation, EQ-HP-6T, Richmond, CA) (HP) in a ~12.7 mm die at a uniaxial compressive stress of ~239 MPa and a temperature of 550°C for 5 minutes. Composites were allowed to cool in the HP to room temperature (RT) before characterization. Novel Al-Sn-matrix composites were designed by adding 35 vol% Ti₃SiC₂, 65 vol% metal. Following composites were fabricated: (a) 0 vol% Sn – 35 vol% Ti₃SiC₂ -65 vol% Al(0Sn-35Ti₃SiC₂-65 Al), (b) 0.5 vol% Sn –35 vol% Ti₃SiC₂ - 64.5 vol% Al(Ti₃SiC₂(35)-Al(64.5)-Sn(0.5)), (c) 1 vol% Sn –35 vol% Ti₃SiC₂ -64 vol% Al(Ti₃SiC₂(35)-Al(64)-Sn(1)), (d) 2 vol% Sn - 35 vol% Ti₃SiC₂ -63 vol% Al(Ti₃SiC₂(35)-Al(63)-Sn(2)), and (e) 5 vol% Sn - 35 vol% Ti₃SiC₂ -60 vol% Al(Ti₃SiC₂(35)-Al(60)-Sn(5)).

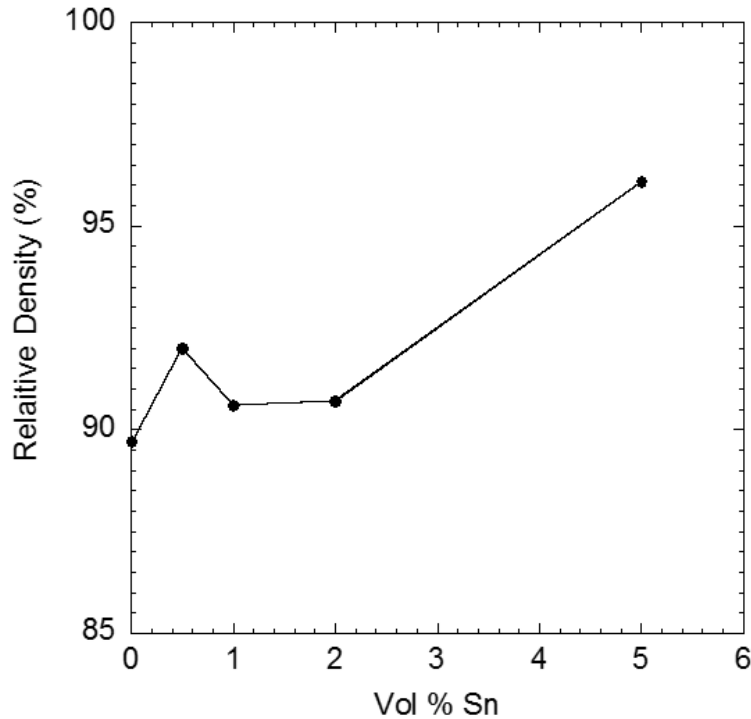


Figure 5.1. Relative density of HP Al-Sn-MAX

In Figure 5.1, the relative density is plotted of a new composite, containing Ti_3SiC_2 (35), Sn(0-5), Al(Bal). The relative densities of these composites are very high in comparison to in Chapter 2, where it was reported that Ti_3SiC_2 (35)-Al(65) was only 73% dense. By the addition of Sn in the system, and using hot pressing for the manufacturing method, it is possible to fabricate composites over 95% dense. For a direct visual comparison, Figure 5.2 shows the porosity in the composites for the three different manufacturing methods of the Al-matrix composites. It is clearly shown that by adding Sn to the system, the porosity is greatly reduced even with the higher concentrations of MAX phase.

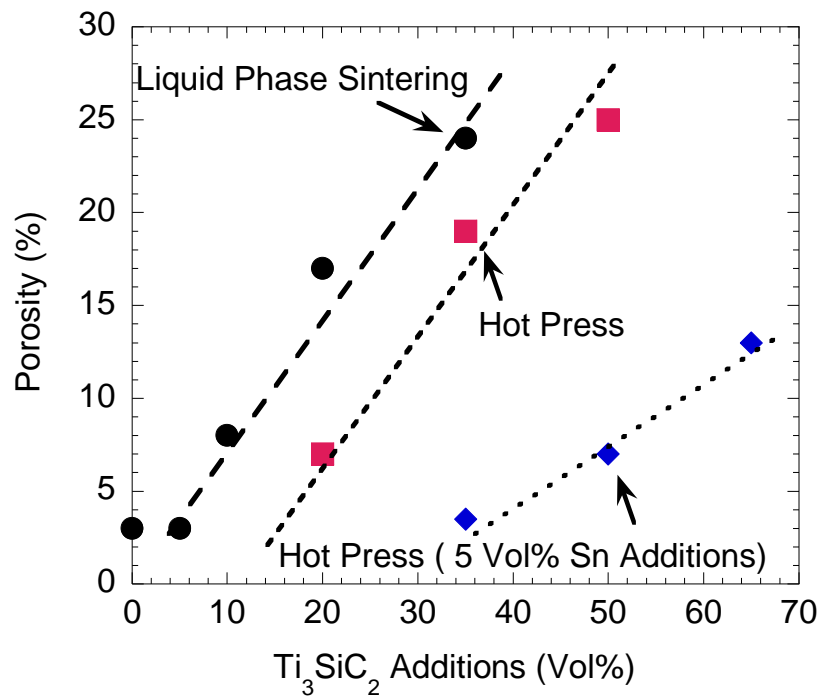


Figure 5.2. Various manufacturing methods' effect on porosity.

It is also shown in Figure 5.2 that by hot pressing it is possible to fabricate composites with much higher MAX phase content than by LPS, allowing for the study of ceramic matrix composites (CMC). This would be an excellent area of research to continue to explore. In this thesis, only metal matrix composites were studied extensively, and it has shown very promising results. The author would recommend that this work is continued to be funded to explore the CMC properties of the work conducted here.

APPENDIX

APPENDIX

Status of journal publications

1. “Development of Novel Multifunctional MAX-Al Composites”, S. Gupta, T. Hammann, and R. Johnson (Accepted for publication, Journal of Materials Engineering and Performance - Manuscript ID JMEP-14-09-7049.R1).
2. “Novel Sn Matrix Composites Reinforced with Ti_3SiC_2 (nanolaminates) Particulates”, T. Hammann, R. Johnson, and S. Gupta (to be submitted)
3. “Novel Multifunctional MAX-Epoxy Composites”, S. Gupta, T. Hammann, and R. Johnson (Accepted for publication, Tribology Transactions - Manuscript UTRB-1581.R1).

Contributed presentations during Master’s degree

1. “Novel MAX (Nanolaminates) -Al (Aluminum) Multifunctional Composites”, T. Hammann*, S. Gupta, R Johnson, M Riyad, (MS&T, 2014).
2. “Novel Methods for Manufacturing Porous Ceramics”, S. Gupta, M. Riyad*, T. Hammann, R. Johnson, (MS&T, 2014).
3. “On the Development of Novel Light Weight Multifunctional Composites”, S. Gupta, R. Johnson, T. Hammann*, M Riyad, (MS&T, 2014).
4. “On the Development of Next Generation Green Manufacturing Technologies”, S. Gupta*, M. Riyad, T. Hammann, R. Johnson, (MS&T, 2014).

5. "Development of Novel MAX-Al Composites" T. Hammann*, R. Johnson, M. F. Riyad, S. Gupta, University of North Dakota, USA. 2014 Scholarly Forum, University of North Dakota (2014).
6. "On the Development of Novel MAX-Al Composites" T. Hammann*, R. Johnson, M. F. Riyad, S. Gupta, University of North Dakota, USA. 36th International Conference and Expo on Advanced Ceramics and Composites (ICACC'14). Daytona Beach, Fl. (2014).
7. "Tribology of Novel MAX-Al Composites" R. Johnson*, T. Hammann, M. F. Riyad, S. Gupta, University of North Dakota, USA. ICACC'14 Daytona Beach, Fl.
8. "Novel Green Manufacturing Technologies" S. Gupta*, M. F. Riyad, T. Hammann, R. Johnson, University of North Dakota, USA. ICACC'14 Daytona Beach, Fl.
9. "Novel Processing Methods for Developing Porous Oxides and Carbide Ceramics" M. F. Riyad*, R. Johnson, T. Hammann, S. Gupta, University of North Dakota, ICACC'14 Daytona Beach, Fl.
10. "On the Manufacturing and Tribology of MAX-Al Composites" T. Hammann*, R. Johnson*, M. F. Riyad, S. Gupta, University of North Dakota Engineering Seminar Series. (2013).
11. "Novel Low Alkali Activated Fly Ash Cement (LAFAC) based Composites" M. F. Riyad, T. Hammann, R. Johnson and S. Gupta, University of North Dakota, USA. 4th Advances in Cement-based Materials, UIUC, (2013)

12. “On the Development of Low Alkali Activated Fly Ash Cement (LAFAC)” Surojit
Gupta, M. Faisal Riyad, Ryan Johnson and Tom Hammann, University of North
Dakota, USA. UIUC, (2013)

REFERENCES

Chapter 1

1. Barsoum MW, El-Raghy T. 2000. The MAX phases: unique new carbide and nitride materials. *Am. Sci.* **89**:336–45
2. "Research." In *Materials*. Drexel University, n.d. Web. 10 Jan. 2013.
3. Barsoum MW. 2000. The MN+1AXN phases: a new class of solids; thermodynamically stable nanolaminates. *Prog. Solid State Chem.* **28**:201–81
4. Barsoum MW, Zhen T, Kalidindi SR, Radovic M, Murugahiah A. 2003. Fully reversible, dislocation based compressive deformation of Ti_3SiC_2 to 1 GPa. *Nat. Mater.* **2**:107–11
5. Barsoum MW, Radovic M. 2011, Elastic and Mechanical Properties of the MAX phase. *Annual Review of Materials Research.* **41**:195-227
6. Nowotny, H. (1970) *Prog. Solid State Chem.*, 2, 27
7. Jeitschko, W. and Nowotny, H. (1967) *Monatsh. Chem.*, **98**,329
8. Wolfsgruber H., Nowotny, H., and Benesovsky, F. (1967) *Monatsh. Chem*, **98**, 2401
9. Pietzka, M.A. and Schuster, J. (1994) *J. Phase Equilib*, **15**, 392
10. Dubois, S. Cabioch, T. (2007) *J. Am Ceram. Soc*, **90**, 2642
11. Etzkorn, J. Ande, M. and Hillebrecht, H. (2007) *Inorg. Chem.*, **46**, 1410
12. Rawn, C.J. et al, (2000) *Mater. Res. Bull*, **35**, 1785

13. Hu, C. et al. (2007) Scripta Mater, **57**, 893
14. “Cu/ Ti₃SiC₂ composite: a new electrofriction material”, Y. Zhang, Z.M. Sun, Y.C. Zhou, Mater. Res. Innov. **3** 80–84 (1999).
15. “Ta₂AlC and Cr₂AlC Ag-based composites - New solid lubricant materials for use over a wide temperature range against Ni-based superalloys and alumina”, S. Gupta, D. Filimonov, T. Palanisamy, T. El-Raghy and M. W. Barsoum, Wear **262**, 1479-1489 (2007).
16. “Nanocrystalline M-matrix composites with ultrahigh damping properties”, B. Anasori, S. Amini, V. Presser, and M. W. Barsoum, Magnesium Technology 2011, John Wiley and Sons, Inc, 463-468 (2011).
17. “Powder metallurgy processing and compressive properties of Ti₃AlC₂/Al composites”, W.J. Wang, V. Gauthier-Brunet, G.P. Bei, G. Laplanche, J. Bonneville, A. Joulain, S. Dubois, Mater. Sci. Eng. **A 530**, 168–173 (2011).
18. “Current-activated, pressure-assisted infiltration: a novel, versatile route for producing interpenetrating ceramic–metal composites”, L. Hu, A. Kothalkar, M. O’Neil, I. Karaman, M. Radovic, Mater. Res. Lett. (2014),
<http://dx.doi.org/10.1080/21663831.2013.873498>.
19. “Thermo-mechanical response and damping behavior of shape memory alloy/MAX phase composites”, A. Kothalkar, R. Benitez, L. Hu, M. Radovic, I. Karaman, , Metall. Mater. Trans. A. **45**, 2646–2658 (2014).
20. “Engineering Materials Properties and Selection”, K. G. Budinski and M. K. Budinski, Prentice Hall, 9th Edition (2010).

21. “Metal matrix composites – From science to technological significance”, D.B. Miracle, Composites Science and Technology **65**, 2526–2540 (2005).
22. “Microstructural evolution of reactive-sintered aluminum matrix composites”, Z Chen, T. Takeda, K. Ikeda, Composites Science and Technology **68**, 2245–2253 (2008).
23. “Machining of metal matrix composites: Effect of ceramic particles on residual stress, surface roughness and chip formation”, A. Pramanik, L.C. Zhang, J.A. Arsecularatne, International Journal of Machine Tools & Manufacture **48** 1613–1625 (2008).
24. “Machining of Al/SiC particulate metal-matrix composites, Part I: tool performance”, M. El-Gallab, M. Sklad, Journal of Materials Processing Technology, **83** 151–158 (1998).
25. “Evaluation of machining performance of MMC with PCBN and PCD tools”, X. Ding, W.Y.H. Liew, X.D. Liu Wear, **259** 1225–1234 (2005).

Chapter 2

1. “Elastic and Mechanical Properties of the MAX Phases”, M.W. Barsoum and M. Radovic Annu. Rev. Mater. Res. **41**, 195-227 (2011).
2. “Synthesis and characterization of a remarkable ceramic: Ti_3SiC_2 ”, M.W. Barsoum, T. El-Raghy, J. Am. Ceram. Soc. **79**, 1953–1956 (1996).
3. M.W. Barsoum, The $M_{n+1}AX_n$ phases: a new class of solids; thermodynamically stable nanolaminates, Prog. Solid State Chem. **28**, 201–281 (2000).
4. S. Amini, M.W. Barsoum, T. El-Raghy, Synthesis and mechanical properties of

- fully dense Ti_2SC , J. Am. Ceram. Soc. **90** (12), 3953–3958 (2007).
5. “Effect of temperature, strain rate and grain size on the mechanical response of Ti_3SiC_2 in Tension”, M. Radovic, M.W. Barsoum, T. El-Raghy, S.M. Wiederhorn, W.E. Luecke,, Acta Mater. **50**, 1297–1306 (2002).
 6. “Processing and mechanical properties of Ti_3SiC_2 . II. Effect of grain size and deformation temperature”, T El-Raghy, M.W. Barsoum, A. Zavaliangos, S.R. Kalidindi, J. Am. Ceram.Soc. **82**, 2855–2860 (1999).
 7. “Compressive creep of fine and coarse-grained Ti_3SiC_2 in air in the 1100–1300 °C temperature range”, T. Zhen, M.W. Barsoum, S.R. Kalidindi, M. Radovic, Z.M. T. El-Raghy, Acta Mater. **53**, 4963–4973 (2005).
 8. “Oxidation behavior of Ti_3SiC_2 at high temperature in air” S.B. Li, L.F. Cheng, L.T. Zhang, Mater. Sci. Eng. Struct. Mater. Prop. Microstruct. Process. **341**, 112–120 (2003).
 9. “Synthesis and oxidation of V_2AlC and $(Ti_{0.5},V_{0.5})_2AlC$ in air”, S. Gupta, M.W. Barsoum, , J. Electrochem. Soc. **151**, D24–D29 (2004).
 10. “Oxidation of $Ti_{n+1}AlX_n$ ($n = 1–3$ and $X = C, N$). II. Experimental results”, M.W. Barsoum, N. Tzenov, A. Procopio, T. El-Raghy, M. Ali, J. Electrochem. Soc. **148**, C551–C562 (2001).
 11. “Oxidation behavior of Ti_3AlC_2 powders in flowing air”, X.H. Wang, Y.C. Zhou, , J. Mater. Chem. **12** (9), 2781–2785 (2002).
 12. “Isothermal oxidation of Ta_2AlC in air”, S. Gupta, D. Filimonov, M.W. Barsoum, J. Am. Ceram. Soc. **89**, 2974–2976 (2006).
 13. “High-temperature oxidation and hot corrosion of Cr_2AlC ”, Z.J. Lin, M.S. Li, J.Y. Wang, Y.C. Zhou, Acta Mater. **55**, 6182–6191 (2007).

14. "On the tribology of the MAX phases and their composites during dry sliding: A review", S.Gupta and M.W. Barsoum, *Wear* **271**, 1878– 1894 (2011).
15. "Cu/Ti₃SiC₂ composite: a new electrofriction material", Y. Zhang, Z.M. Sun, Y.C. Zhou, *Mater. Res. Innov.* **3** 80–84 (1999).
16. "Ta₂AlC and Cr₂AlC Ag-based composites - New solid lubricant materials for use over a wide temperature range against Ni-based superalloys and alumina", S. Gupta, D. Filimonov, T. Palanisamy, T. El-Raghy and M. W. Barsoum, *Wear* **262**, 1479-1489 (2007).
17. "Nanocrystalline M-matrix composites with ultrahigh damping properties", B. Anasori, S. Amini, V. Presser, and M. W. Barsoum, *Magnesium Technology 2011*, John Wiley and Sons, Inc, 463-468 (2011).
18. "Powder metallurgy processing and compressive properties of Ti₃AlC₂/Al composites", W.J. Wang, V. Gauthier-Brunet, G.P. Bei, G. Laplanche, J. Bonneville, A. Joulain, S. Dubois, *Mater. Sci. Eng. A* **530**, 168–173 (2011).
19. "Current-activated, pressure-assisted infiltration: a novel, versatile route for producing interpenetrating ceramic–metal composites", L. Hu, A. Kothalkar, M. O'Neil, I. Karaman, M. Radovic, *Mater. Res. Lett.* (2014), <http://dx.doi.org/10.1080/21663831.2013.873498>.
20. "Thermo-mechanical response and damping behavior of shape memory alloy/MAX phase composites", A. Kothalkar, R. Benitez, L. Hu, M. Radovic, I. Karaman, *Metall. Mater. Trans. A*. **45**, 2646–2658 (2014).
21. "Engineering Materials Properties and Selection", K. G. Budinski and M. K. Budinski, Prentice Hall, 9th Edition (2010).

22. “Metal matrix composites – From science to technological significance”, D.B. Miracle, Composites Science and Technology **65**, 2526–2540 (2005).
23. “Microstructural evolution of reactive-sintered aluminum matrix composites”, Z Chen, T. Takeda, K. Ikeda, Composites Science and Technology **68** 2245–2253 (2008).
24. “Machining of metal matrix composites: Effect of ceramic particles on residual stress, surface roughness and chip formation”, A. Pramanik, L.C. Zhang, J.A. Arsecularatne, International Journal of Machine Tools & Manufacture **48** 1613–1625 (2008).
25. “Machining of Al/SiC particulate metal-matrix composites, Part I: tool performance”, M. El-Gallab, M. Sklad, Journal of Materials Processing Technology, **83** 151–158 (1998).
26. “Evaluation of machining performance of MMC with PCBN and PCD tools”, X. Ding, W.Y.H. Liew, X.D. Liu Wear, **259** 1225–1234 (2005).

Chapter 3

1. “Elastic and Mechanical Properties of the MAX Phases”, M.W. Barsoum and M. Radovic Annu. Rev. Mater. Res. **41**, 195-227 (2011).
2. “Synthesis and characterization of a remarkable ceramic: Ti_3SiC_2 ”, M.W. Barsoum, T. El- Raghy, J. Am. Ceram. Soc. **79**, 1953–1956 (1996).
3. M.W. Barsoum, The $M_{n+1}AX_n$ phases: a new class of solids; thermodynamically
4. stable nanolaminates, Prog. Solid State Chem. **28**, 201–281 (2000).

5. S. Amini, M.W. Barsoum, T. El-Raghy, Synthesis and mechanical properties of
6. fully dense Ti_2SC , J. Am. Ceram. Soc. **90** (12), 3953–3958 (2007).
7. “Effect of temperature, strain rate and grain size on the mechanical response of Ti_3SiC_2 in Tension”, M. Radovic, M.W. Barsoum, T. El-Raghy, S.M. Wiederhorn, W.E. Luecke,, Acta Mater. **50**, 1297–1306 (2002).
8. “Processing and mechanical properties of Ti_3SiC_2 . II. Effect of grain size and deformation temperature”, T El-Raghy, M.W. Barsoum, A. Zavaliangos, S.R. Kalidindi, J. Am. Ceram.Soc. **82**, 2855–2860 (1999).
9. “Compressive creep of fine and coarse-grained Ti_3SiC_2 in air in the 1100–1300 °C
10. temperature range”, T. Zhen, M.W. Barsoum, S.R. Kalidindi, M. Radovic, Z.M. T. El-
11. Raghy, Acta Mater. **53**, 4963–4973 (2005).
12. “Oxidation behavior of Ti_3SiC_2 at high temperature in air” S.B. Li, L.F. Cheng, L.T. Zhang, Mater. Sci. Eng. Struct. Mater. Prop. Microstruct. Process. **341**, 112–120 (2003).
13. “Synthesis and oxidation of V_2AlC and $(Ti_{0.5},V_{0.5})_2AlC$ in air”, S. Gupta, M.W. Barsoum, , J. Electrochem. Soc. **151**, D24–D29 (2004).
14. “Oxidation of $Ti_{n+1}AlX_n$ ($n = 1–3$ and $X = C, N$). II. Experimental results”, M.W. Barsoum, N. Tzenov, A. Procopio, T. El-Raghy, M. Ali, J. Electrochem. Soc. **148**, C551–C562 (2001).

15. "Oxidation behavior of Ti_3AlC_2 powders in flowing air", X.H. Wang, Y.C. Zhou, , J.
16. Mater. Chem. **12** (9), 2781–2785 (2002).
17. "Isothermal oxidation of Ta_2AlC in air", S. Gupta, D. Filimonov, M.W. Barsoum, J.
18. Am. Ceram. Soc. **89**, 2974–2976 (2006).
19. "High-temperature oxidation and hot corrosion of Cr_2AlC ", Z.J. Lin, M.S. Li, J.Y. Wang, Y.C. Zhou, Acta Mater. **55**, 6182–6191 (2007).
20. "On the tribology of the MAX phases and their composites during dry sliding: A review", S.Gupta and M.W. Barsoum, Wear **271**, 1878– 1894 (2011).
21. "Cu/ Ti_3SiC_2 composite: a new electrofriction material", Y. Zhang, Z.M. Sun, Y.C. Zhou, Mater. Res. Innov. **3** 80–84 (1999).
22. " Ta_2AlC and Cr_2AlC Ag-based composites - New solid lubricant materials for use over a wide temperature range against Ni-based superalloys and alumina", S. Gupta, D. Filimonov, T. Palanisamy, T. El-Raghy and M. W. Barsoum, Wear **262**, 1479-1489 (2007).
23. "Nanocrystalline M-matrix composites with ultrahigh damping properties", B. Anasori, S. Amini, V. Presser, and M. W. Barsoum, Magnesium Technology 2011, John Wiley and Sons, Inc, 463-468 (2011).
24. "Powder metallurgy processing and compressive properties of Ti_3AlC_2/Al composites", W.J. Wang, V. Gauthier-Brunet, G.P. Bei, G. Laplanche, J. Bonneville, A. Joulain, S. Dubois, Mater. Sci. Eng. **A 530**, 168–173 (2011).

25. “Current-activated, pressure-assisted infiltration: a novel, versatile route for producing interpenetrating ceramic–metal composites”, L. Hu, A. Kothalkar, M. O’Neil, I. Karaman, M. Radovic, *Mater. Res. Lett.* (2014), <http://dx.doi.org/10.1080/21663831.2013.873498>.
26. “Thermo-mechanical response and damping behavior of shape memory alloy/MAX phase composites”, A. Kothalkar, R. Benitez, L. Hu, M. Radovic, I. Karaman, , *Metall. Mater. Trans. A.* **45**, 2646–2658 (2014).
27. “Engineering Materials Properties and Selection”, K. G. Budinski and M. K. Budinski, Prentice Hall, 9th Edition (2010).
28. “Metal matrix composites – From science to technological significance”, D.B. Miracle, *Composites Science and Technology* **65**, 2526–2540 (2005).
29. “Microstructural evolution of reactive-sintered aluminum matrix composites”, Z Chen, T. Takeda, K. Ikeda, *Composites Science and Technology* **68** 2245–2253 (2008).
30. “Machining of metal matrix composites: Effect of ceramic particles on residual stress, surface roughness and chip formation”, A. Pramanik, L.C. Zhang, J.A. Arsecularatne, *International Journal of Machine Tools & Manufacture* **48** 1613–1625 (2008).

Chapter 4

1. M.W. Barsoum, M. Radovic, in: R.W.C.K.H.J. Buschow, M.C. Flemings, E.J. Kramer, S. Mahajan, P. Veysiere (Eds.), *Encyclopedia of Materials Science and Technology*,

Elsevier, Amsterdam, 2004.

2. "Synthesis and characterization of a remarkable ceramic: Ti_3SiC_2 ", M.W. Barsoum, T. El-Raghy, J. Am. Ceram. Soc. 79 (1996) 1953–1956.
3. M.W. Barsoum, The $M_{n+1}AX_n$ phases: a new class of solids; thermodynamically stable nanolaminates, Prog. Solid State Chem. 28 (2000) 201–281.
4. S. Amini, M.W. Barsoum, T. El-Raghy, Synthesis and mechanical properties of fully dense Ti_2SC , J. Am. Ceram. Soc. 90 (12) (2007) 3953–3958.
5. "Effect of temperature, strain rate and grain size on the mechanical response of Ti_3SiC_2 in Tension", M. Radovic, M.W. Barsoum, T. El-Raghy, S.M. Wiederhorn, W.E. Luecke, Acta Mater. 50 (2002) 1297–1306.
6. "Processing and mechanical properties of Ti_3SiC_2 . II. Effect of grain size and deformation temperature", T El-Raghy, M.W. Barsoum, A. Zavaliangos, S.R. Kalidindi, J. Am. Ceram. Soc. **82** (1999) 2855–2860.
7. "Compressive creep of fine and coarse-grained Ti_3SiC_2 in air in the 1100–1300 °C temperature range", T. Zhen, M.W. Barsoum, S.R. Kalidindi, M. Radovic, Z.M. Sun, T. El-Raghy, Acta Mater. 53 (2005) 4963–4973.
8. "Oxidation behavior of Ti_3SiC_2 at high temperature in air" S.B. Li, L.F. Cheng, L.T. Zhang, Mater. Sci. Eng. Struct. Mater. Prop. Microstruct. Process. **341**, 112–120 (2003).
9. "Synthesis and oxidation of V_2AlC and $(Ti_{0.5}, V_{0.5})_2AlC$ in air", S. Gupta, M.W. Barsoum, J. Electrochem. Soc. 151 (2004) D24–D29.
10. "Oxidation of $Ti_{n+1}AlX_n$ ($n = 1-3$ and $X = C, N$). II. Experimental results", M.W. Barsoum, N. Tzenov, A. Procopio, T. El-Raghy, M. Ali, J. Electrochem. Soc. **148**, C551–C562 (2001).
11. "Oxidation behavior of Ti_3AlC_2 powders in flowing air", X.H. Wang, Y.C. Zhou, J. Mater. Chem. 12 (9) (2002) 2781–2785.

12. “Isothermal oxidation of Ta₂AlC in air”, S. Gupta, D. Filimonov, M.W. Barsoum, J. Am. Ceram. Soc. **89**, 2974–2976 (2006).
13. “High-temperature oxidation and hot corrosion of Cr₂AlC”, Z.J. Lin, M.S. Li, J.Y. Wang, Y.C. Zhou, Acta Mater. **55**, 6182–6191 (2007).
14. “On the tribology of the MAX phases and their composites during dry sliding: A review”, S. Gupta and M.W. Barsoum, Wear **271**, 1878– 1894 (2011).
15. “MAX phases as solid lubricant materials”, S. Gupta, T. Palanisamy, M.W. Barsoum and C.W. Li, (U.S Patent 7,553,564 BA, June 30, 2009).
16. “MAX Phases with additives as solid lubricant materials”, T. Palanisamy, S. Gupta, C. W. Li and M. W. Barsoum, (US Patent 7.572,313 B2, Aug. 11, 2009).
17. “Tribological behavior of select MAX phases against Al₂O₃ at elevated temperatures”, S. Gupta, D. Filimonov, T. Palanisamy and M. W. Barsoum, Wear **265**, 560-565 (2008).
18. “Ambient and 550°C tribological behavior of select MAX phases against Ni-based superalloys”, S. Gupta, D. Filimonov, V. Zaitsev, T. Palanisamy and M. W. Barsoum, Wear **264**, 270-278 (2008).
19. “Tribology of Ti₂SC – a novel MAX Phase”, S. Gupta, D. Filiminov, T. Palanisamy, T. El-Raghy and Michel. W. Barsoum, J. Am. Ceram. Soc. **90**, 3566-3571 (2007).
20. “Ta₂AlC and Cr₂AlC Ag-based composites - New solid lubricant materials for use over a wide temperature range against Ni-based superalloys and alumina”, S. Gupta, D. Filimonov, T. Palanisamy, T. El-Raghy and M. W. Barsoum, Wear **262**, 1479-1489 (2007).
21. “Study of tribofilms formed during dry sliding of Ta₂AlC/Ag or Cr₂AlC/Ag composites against Ni-base superalloys and Al₂O₃”, S. Gupta, D. Filimonov, V. Zaitsev, T. Palanisamy, T. El-Raghy, M.W. Barsoum, Wear **267**, 1490-1500

- (2009).
22. “Chameleon coatings: Adaptive surfaces to reduce friction and wear in extreme environments C. Muratore”, A.A. Voevodin, *Annu. Rev. Mater. Res.* **39** 297–324 (2009).
 23. “Processing, microstructural characterization and mechanical properties of a Ti₂AlC/nanocrystalline Mg-matrix composite”, S. Amini, C. Ni, M. W. Barsoum, *Comp. Sci. and Tech.* **69**, 414–420 (2009).
 24. “Nanocrystalline M-matrix composites with ultrahigh damping properties”, B. Anasori, S. Amini, V. Presser, and M. W. Barsoum, *Magnesium Technology 2011*, John Wiley and Sons, Inc, 463-468 (2011).
 25. “On the effect of texture on the mechanical and damping properties of nanocrystalline Mg-matrix composites reinforced with MAX phases”, S. Amini, M. W. Barsoum, *Mat. Sci.& Eng. A* **527**, 3707-3718 (2010).
 26. “Investigation of the wear behaviour of a glass–fiber reinforced composite and plain polyester resin”, P. Hasim, T. Nihat, *Compos Sci Technol* **62**, 367–70 (2002).
 27. “Abrasive wear behaviour of hard powders filled glass fabric–epoxy hybrid composites”, N. Mohan, S. Natarajan, S.P. Kumaresh Babu, *Materials and Design* **32**, 1704–1709 (2011).
 28. “Tribological properties of epoxy nanocomposites I. Enhancement of the wear resistance by nano-TiO₂ particles”, L. Chang, Z. Zhang, C. B. K. Friedrich, *Wear* **258**, 141–148 (2005).
 29. “Tribological properties of epoxy nanocomposites III. Characteristics of transfer films”, L. Changa, Z. Zhang, L. Ye, K. Friedrich, *Wear* **262**, 699–706 (2007).
 30. “Dry sliding wear characteristics of glass–epoxycomposite filled with silicon carbide and graphite particles S. Basavarajappa, S.Ellangovan, *Wear* **296**, 491–496 (2012).

31. “Enhancement effect of nanoparticles on the sliding wear of short fiber-reinforced polymer composites: A critical discussion of wear mechanisms”, L. Chang , K. Friedrich, Tribology International **43**, 2355–2364 (2010).
32. “A graphite nanoplatelet/epoxy composite with high dielectric constant and high thermal conductivity”, C. Min, D. Yu, J. Cao, G. Wang, L. Feng, Carbon **55**, 116–125 (2013).
33. “Self-lubricating properties of PTFE/serpentine nanocomposite against steel at different loads and sliding velocities”, Z. Jia, Y. Yanga, Composites: Part B **43**, 2072–2078 (2012).
34. “Sliding wear performance of nano-SiO₂/short carbon fiber/epoxy hybrid composites”, Q. B. Guoa, M. Z. Rong, G. Liang Jia, K. T. Lau, M. Q. Zhang, Wear **266**, 658–665 (2009).
35. T. El-Raghy, P. Blau, M.W. Barsoum, Effect of grain size on friction and wear behavior of Ti₃SiC₂, Wear 238 (2) (2000) 125–130.
36. “Tribological duality of Ti₃SiC₂”, A. Souchet, J. Fontaine, M. Belin, T. Le Mogne, J.-L. Loubet, M.W. Barsoum, Tribol. Lett. **18**, 341–352 (2005).
37. “Tribology of MAX phases and their composites”, S. Gupta, PhD Thesis, Drexel University (2006).
38. S. Myhra, J.W.B. Summers, E.H. Kisi, Ti₃SiC₂ – a layered ceramic exhibiting ultralow friction, Mater. Lett. Mater. Lett. 39 (1999) 6–11.
39. Y. Zhang, G.P. Ding, Y.C. Zhou, B.C. Cai, Ti₃SiC₂ – a self-lubricating ceramic, Mater. Lett. 55 (2002) 285–289.